ARTICLE

The E3 ligase COP1 promotes ERα signaling and suppresses EMT in breast cancer

Seng Chuan Tang[1,2], Quentin Lion[1,2], Olivier Peulen[1,3], Philippe Chariot[1,2], Arnaud Lavergne[1,4], Alice Mayer[1,4], Paula Allepuz Fuster[1,2], Pierre Close[1,5,6], Sebastian Klein[7], Alexandra Florin[7], Reinhard Büttner[7], Ivan Nemazanyy[8], Kateryna Shostak[1,2,9] and Alain Chariot[1,2,6,9]✉

ERα signaling drives proliferation, survival and cancer initiation in the mammary gland. Therefore, it is critical to elucidate mechanisms by which ERα expression is regulated. We show that the tumor suppressor E3 ligase COP1 promotes the degradative polyubiquitination of the microtubule-associated protein HPIP. As such, COP1 negatively regulates estrogen-dependent AKT activation in breast cancer cells. However, COP1 also induces ERα expression and ERα-dependent gene transcription, at least through c-Jun degradation. COP1 and ERα levels are positively correlated in clinical cases of breast cancer. COP1 also supports the metabolic reprogramming by estrogens, including glycolysis. On the other hand, COP1 suppresses EMT in breast cancer cells. COP1 deficiency also contributes to Tamoxifen resistance, at least through protective autophagy. Therefore, COP1 acts as an oncogenic E3 ligase by promoting ERα signaling but also acts as a tumor suppressor candidate by preventing EMT, which reflects a dual role of COP1 in breast cancer.

Oncogene (2022) 41:173–190; https://doi.org/10.1038/s41388-021-02038-3

INTRODUCTION

About 70% of breast cancer are positive for ERα expression and therefore rely on hormonal growth and are responsive to adjuvant anti-estrogenic therapies [1]. ERα is a nuclear receptor superfamily member and moves into the nucleus upon estrogen stimulation in order to induce the expression of target genes such as *Cyclin D1*, *GREB1*, and *c-MYC* [2–5]. As a result, ERα signaling is defined as a critical pathway for cancer initiation and proliferation in a majority of breast malignancies [6].

ERα expression is tightly regulated, both at the transcriptional and post-transcriptional levels. ERα transcription is regulated by at least nine distinct promoters harboring multiple binding sites for several transcription factors [7]. Transcription factors which control ERα transcription in breast cancer cells include ERBF-1, AP2α/γ, FOXO3a, FOXM1, and GATA-3 among others [8–12]. c-Jun/c-Fos belong to the very few transcription factors defined as negative regulators of ERα transcription [13, 14]. Multiple post-translational mechanisms that regulate ERα expression and stability have been described [15]. In this context, HPIP (also referred to as PBXIP1) assembles a signaling complex to connect the p85 subunit of PI3K and ERα to microtubules in order to properly activate AKT in response to estrogens [16]. HPIP stabilizes ERα in breast cancer cells and promotes estrogen-dependent AKT activation [16]. The E3 ligase MDM2, which targets HPIP for degradation, indirectly destabilizes ERα [17].

In a search for E3 ligases that target HPIP for degradation, we identified COP1, a candidate originally identified in a light signaling pathway in plants [18]. COP1 possesses some intrinsic E3 ligase activity and also triggers the degradation of substrates such as c-Jun and ETS transcription factors by linking them to the Cullin 4A-DDB1-RBX1-DET1 ligase complex through a direct association with DET1 [19–21]. We show here that COP1 polyubiquitinates and degrades HPIP but promotes ERα expression, at least through c-Jun degradation. Likewise, COP1 and ERα levels are positively correlated in clinical cases of breast cancer. COP1 also promotes metabolic reprogramming by estrogens and supports glycolysis. Finally, COP1 also prevents EMT in breast cancer cells through an ERα-independent pathway. Taken together, our data define molecular mechanisms by which COP1 acts as a positive regulator of ERα signaling and also as a negative regulator of EMT, which reflects a dual role of COP1 in breast cancer.

RESULTS

COP1 binds and polyubiquitinates HPIP

MDM2 promotes HPIP polyubiquitination and degradation through a TBK1-dependent pathway [17]. Our siRNA-based screening defined other candidates that negatively regulate HPIP protein levels. Indeed, COP1 deficiency enhanced HPIP levels in

[1]Interdisciplinary Cluster for Applied Genoproteomics, University of Liege, CHU, Sart-Tilman, Liège, Belgium. [2]Laboratory of Medical Chemistry, GIGA Stem Cells, University of Liege, CHU, Sart-Tilman, Liège, Belgium. [3]Metastasis Research Laboratory, GIGA Cancer, University of Liege, CHU, Sart-Tilman, Liège, Belgium. [4]GIGA Genomics Platform, University of Liege, CHU, Sart-Tilman, Liège, Belgium. [5]Laboratory of Cancer Signaling, GIGA Stem Cells, University of Liege, CHU, Sart-Tilman, 4000 Liège, Belgium. [6]Walloon Excellence in Life Sciences and Biotechnology (WELBIO), Wavres, Belgium. [7]Institute for Pathology-University Hospital of Cologne, Cologne, Germany. [8]Platform for Metabolic Analyses, Structure Fédérative de Recherche Necker, INSERM US24/CNRS UMS 3633, Paris, France. [9]These authors contributed equally: Kateryna Shostak, Alain Chariot. ✉email: Alain.chariot@uliege.ac.be

Received: 31 May 2021 Revised: 14 September 2021 Accepted: 23 September 2021
Published online: 29 October 2021

breast cancer-derived MCF7 cells (Fig. 1a). COP1 bound HPIP, as evidenced by co-immunoprecipitation experiments in HEK293 cells (Fig. 1b and c). The C-terminal part of HPIP was dispensable for this association as the HPIPΔC500 mutant, which lacks the last 500 amino acids, still bound COP1 (Fig. 1b). Moreover, a HPIP mutant lacking serine 147 ("FLAG-HPIP S147A"), a residue targeted by phosphorylation by TBK1 [17], still bound COP1, suggesting that this interaction occurs in a phospho-independent manner (Fig. 1c). HPIP binds COP1 through its N-terminal domain as the HPIPΔN60 HPIP mutant, which lacks the first 60 amino acids, failed to bind COP1 (Fig. 1c). Likewise, the HPIP mutant lacking the first 150 N-terminal amino acids also failed to bind COP1 (Fig. 1c). COP1 bridges its substrates to DET1 and to a Cullin 4A-containing E3 ligase complex [22]. Consistently, HPIP also bound Cullin 4 A (Supplementary Fig 1a). HPIP mutants lacking its N-terminal part, also bound Cullin 4A, indicating that HPIP associates to COP1 and Cullin 4A through distinct domains (Supplementary Fig 1a). Therefore, the COP1 E3 ligase complex associates with HPIP.

As both MDM2 and COP1 bind HPIP, we next explored whether both E3 ligases may target distinct subpools of HPIP. We biochemically fractionated extracts from MCF7 cells on a sucrose gradient and observed that both COP1 and MDM2 were detected in similar fractions and co-fractionated with HPIP (Supplementary Fig 1b). Therefore, HPIP binds multiple E3 ligase complexes.

We next explored whether COP1 promotes HPIP polyubiquitination. COP1 indeed added polyubiquitin chains on HPIP, similarly to MDM2 (Fig. 1d) [17]. To map the targeted lysine residues, we first tested the COP1-dependent polyubiquitination of several HPIP mutants and found that HPIPΔC250 and HPIPΔC300 mutants were even more polyubiquitinated than wild type HPIP, suggesting that the targeted residues are not located within the last 300 C-terminal amino acids (Fig. 1e). The polyubiquitination chains added on both HPIPΔC350 and HPIPΔC400 mutants were comparable to the ones added on wild type HPIP (Fig. 1e). However, removing the last 450 or 500 amino acids of HPIP severely impaired its polyubiquitination by COP1 (Fig. 1e). Therefore, the COP1-dependent polyubiquitination of HPIP occurs within lysine residues located upstream the last 450/500 C-terminal amino acids. We generated point mutations within HPIP by mutagenesis and noticed that the HPIP K274R but not both HPIP K277 and K293 mutants failed to be properly polyubiquitinated by COP1 (Fig. 1f). Therefore, the lysine K274 of HPIP is the main residue targeted by COP1.

COP1 negatively regulates AKT activation by estrogens

HPIP critically promotes estrogens-dependent signaling pathways as a microtubule-associated protein which binds and stabilizes ERα [16]. Therefore, we explored whether and how COP1 was involved in estrogens-dependent signaling. COP1 deficiency enhanced HPIP protein levels but was dispensable for EGF-dependent AKT activation (Fig. 2a). Estrogens did not impact on COP1 mRNA levels but COP1 deficiency potentiated both TBK1 and AKT activation upon stimulation with estrogens in MCF7 cells (Fig. 2b). Both AKT1 phosphorylation on serine 473 and AKT2 phosphorylation on serine 474 were enhanced upon COP1 deficiency (Fig. 2b and c, respectively). Enhanced HPIP protein levels seen upon COP1 deficiency were also observed in ZR-75 cells, which also express ERα (Fig. 2d). DNA Damage Binding Protein-1 (DDB1) is also part of the COP1-containing E3 ligase complex [22]. COP1 deficiency impaired both DDB1 and Cullin 4 A protein levels in ZR-75 cells, suggesting that COP1 is critical for their stability (Fig. 2d). While HPIP deficiency impaired AKT activation by estrogens in MCF7 cells, COP1 deficiency potentiated AKT activation by estrogens through a HPIP-independent pathway (Fig. 2e). Indeed, cells lacking both HPIP and COP1 still showed enhanced AKT activation by estrogens when compared to control cells (Fig. 2e). Moreover, ERα-negative MDA-MB-231 cells also showed enhanced HPIP protein levels upon COP1 deficiency, indicating that COP1 negatively regulates HPIP levels independently of the ERα status (Fig. 2f). Therefore, COP1 negatively regulates E2-dependent AKT and TBK1 activation in breast cancer cells.

COP1 promotes ERα expression and signaling

COP1 negatively regulates AKT activation by estrogens. At the same time, ERα protein levels were downregulated in COP1-deficient MCF7 cells, which was unexpected as HPIP stabilizes ERα [16, 17] (Fig. 2b). Both ERα and COP1 protein levels were positively correlated in a variety of breast cancer-derived cell lines as well as in patients suffering from an ER^+ breast cancer, which suggests that COP1 promotes ERα expression (Fig. 3a–c, respectively). This has important consequences on ERα signaling as estrogens-dependent ERα phosphorylation was defective upon COP1 deficiency in ZR-75 cells, despite higher HPIP levels (Fig. 3d). Cullin 4A deficiency in MCF7 cells also increased HPIP protein levels and enhanced TBK1 activation by estrogens (Fig. 3e). Moreover, unphosphorylated and phosphorylated ERα protein levels also decreased in Cullin 4A-depleted MCF7 cells (Fig. 3e). DDB1 deficiency in both MCF7 and ZR-75 cells also stabilized HPIP but impaired estrogen-dependent ERα phosphorylation, at least because of decreased ERα levels, similarly to COP1 deficiency (Fig. 3f and g, respectively). COP1 levels were also deregulated upon DDB1 deficiency in both cell lines, indicating that our results are relevant in multiple breast cancer-derived cell lines (Fig. 3f and g). Therefore, members of the COP1 E3 ligase promote ERα expression and signaling.

As p53 drives HPIP transcription [17], we assessed the potential contribution of p53 in HPIP expression upon COP1 deficiency. As expected, p53 mRNA levels were barely detectable in p53-depleted MCF7 cells, even upon COP1 deficiency (Supplementary Fig. 2a). HPIP was still stabilized upon COP1 deficiency in p53-depleted MCF7 cells (Supplementary Fig. 2b). Therefore, p53 is dispensable for HPIP stabilization in COP1-depleted cells. Moreover, ERα protein levels were still downregulated upon COP1 deficiency in these cells, which rules out a role for p53 in the link between COP1 and ERα (Supplementary Fig. 2b). Therefore, the COP1-containing E3 ligase negatively regulates AKT activation by estrogens but nevertheless promotes estrogen signaling, at least by maintaining ERα expression.

The induction of ERα target genes by estrogens relies on COP1

Although COP1 deficiency did not interfere with ERα shuttling into the nucleus upon stimulation with E2, COP1-depleted MCF7 cells nevertheless showed decreased unphosphorylated and phosphorylated ERα nuclear levels (Fig. 4a). As a result, the induction of cell proliferation by estrogens was severely defective upon COP1 deficiency in MCF7 cells, as judged by a decrease percentage of cells in S phase after E2 stimulation upon COP1 deficiency (Fig. 4b). To explore the consequences of COP1 deficiency on the transcriptomic signature induced by estrogens, RNA-Seq and Gene Set Enrichment Analyses (GSEA) were conducted with control and COP1-depleted MCF7 cells stimulated or not with estrogens. An AP1-dependent gene signature was revealed in COP1-depleted MCF7 cells, which is consistent with the stabilization of c-Jun seen upon COP1 deficiency (Supplementary Fig. 3a). These analyses also highlighted a p53-dependent apoptotic signature in COP1-depleted MCF7 cells (Fig. 4c and Supplementary Fig. 3b, respectively), consistent with the destabilization of p53 by COP1 reported in cancer cells [23]. In agreement with a defective ERα expression seen upon COP1 deficiency, COP1-depleted MCF7 cells failed to establish an early and late estrogen-dependent transcriptional signature (Fig. 4d and Supplementary Fig. 3c, respectively). Consistently, estrogens failed to induce mRNA levels of GREB1, an ERα target gene [2], in COP1-depleted MCF7 cells and this conclusion also applied to TSKU and CA12, two other ERα target genes (Fig. 4e). Moreover, the induction of NPY1R, HSP88 and MYB by estrogens was also defective upon

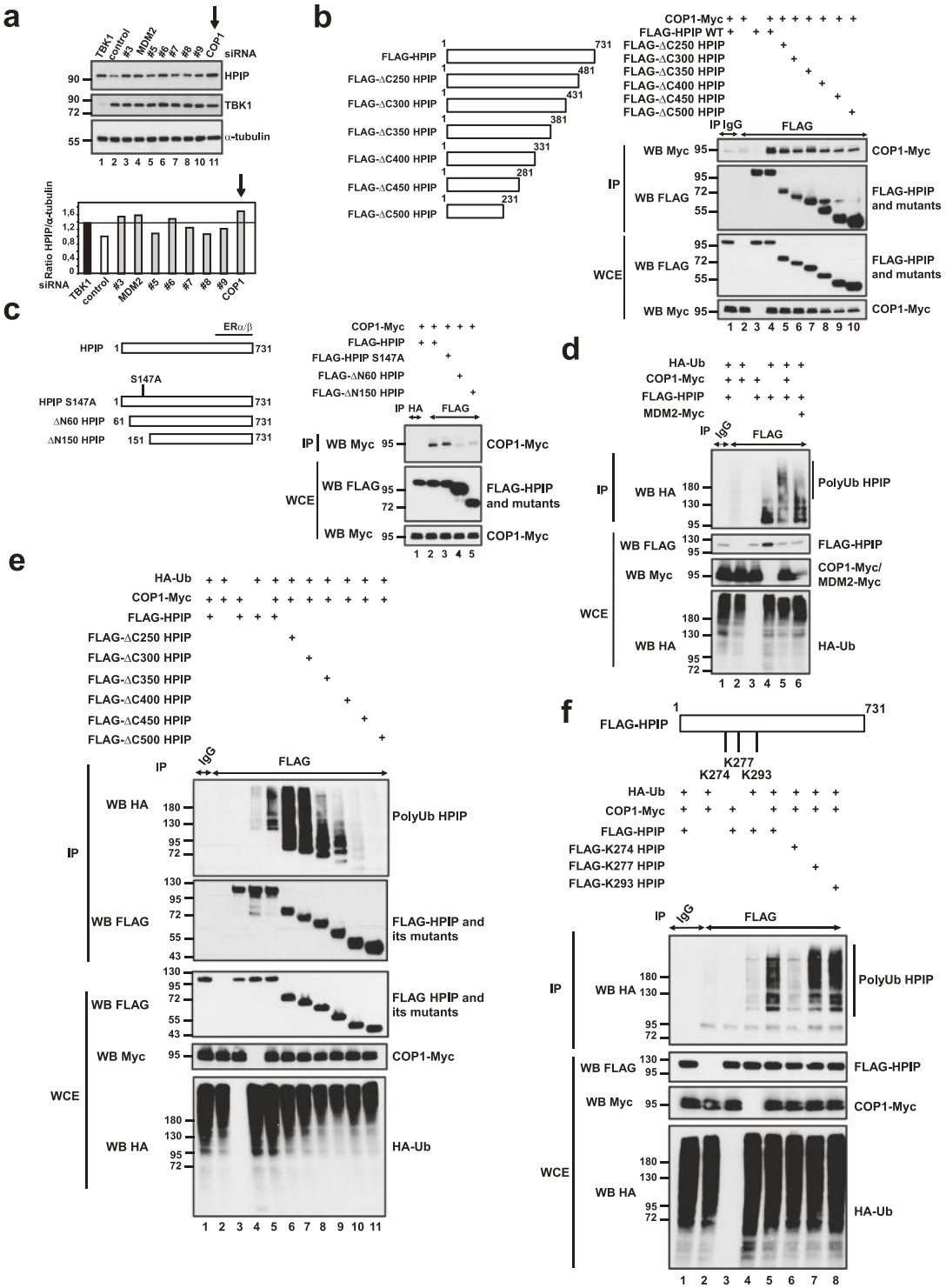

Fig. 1 COP1 binds HPIP. a A siRNA-based screening identified COP1 as an E3 ligase whose depletion in MCF7 cells stabilizes HPIP. The HPIP/α-tubulin ratio in siRNAGFP-transfected MCF7 cells (control) was set to 1 and ratios obtained in other experimental conditions were relative to that (see the histogram). Positive candidates whose siRNA-mediated depletion gives rise to a similar or higher HPIP/α-tubulin ratio than the one obtained in TBK1-depleted cells were selected. **b** and **c** COP1 binds the N-terminal part of HPIP. On the left (**b**), schematic representation of all HPIP constructs tested for binding to HPIP. On the right, HEK293 cells were co-transfected with the indicated expression plasmids and the resulting cell extracts were subjected to anti-FLAG, -IgG **(b)** or -HA **(c)** (negative controls) immunoprecipitations followed by an anti-Myc western blot (WB) (top panel). Whole cell extracts (« WCE ») were also subjected to anti-FLAG and -Myc WBs (bottom panels). The amino acids sequence (from aa 141 to 153) is the domain phosphorylated by TBK1 (**c**). Serine 147 is the main residue of HPIP phosphorylated by TBK1 [17]. **d**–**f** HPIP is polyubiquitinated by COP1. HEK293 cells were co-transfected with the indicated expression plasmids and the resulting cell extracts were subjected to an anti-FLAG or -IgG (negative control) immunoprecipitation followed by an anti-HA WB (top panel) to reveal polyubiquitin chains on HPIP. Whole cell extracts were also subjected to anti-FLAG, -Myc and -HA WBs (bottom panels) using the indicated antibodies.

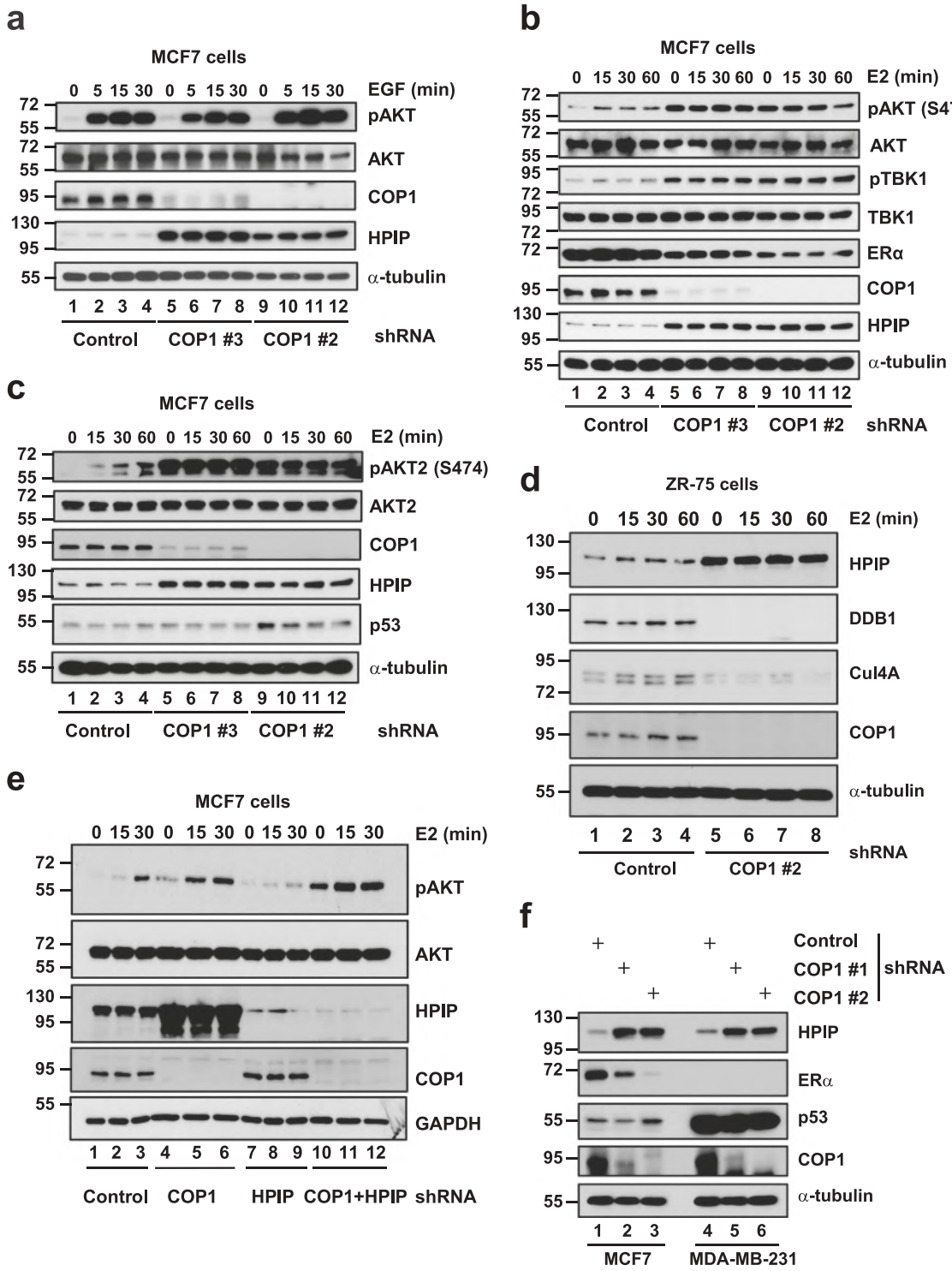

Fig. 2 COP1 negatively regulates estrogens-dependent TBK1 and AKT activation but promotes ERα expression. a COP1 is dispensable for AKT activation by EGF in breast cancer cells. Control or COP1-depleted MCF7 cells were treated or not with EGF (100 ng/ml) for the indicated periods of time and the resulting cell extracts were subjected to WB analyses. **b** and **c** COP1 negatively regulates both TBK1 and AKT1/2 activation by estrogens in breast cancer cells. Control or COP1-depleted MCF7 cells were treated or not with E2 (10 nM) for the indicated periods of time and the resulting cell extracts were subjected to WB analyses. **d** COP1 deficiency in ZR-75 cells enhances HPIP protein levels. Control and COP1-depleted ZR-75 cells were treated or not with E2 (10 nM) for the indicated periods of time and the resulting extracts were subjected to WB analyses using the indicated antibodies. **e** COP1 deficiency enhances estrogens-dependent AKT activation through a HPIP-independent pathway. Control, COP1-, HPIP- or COP1 and HPIP-depleted MCF7 cells were treated or not with E2 (10 nM) for the indicated periods of time and the resulting extracts were subjected to WB analyses. **f** COP1 negatively regulates HPIP protein levels independently of the ERα status. Protein extracts from control and COP1-depleted MCF7 or MDA-MB-231 cells were subjected to WB analyses using the indicated antibodies.

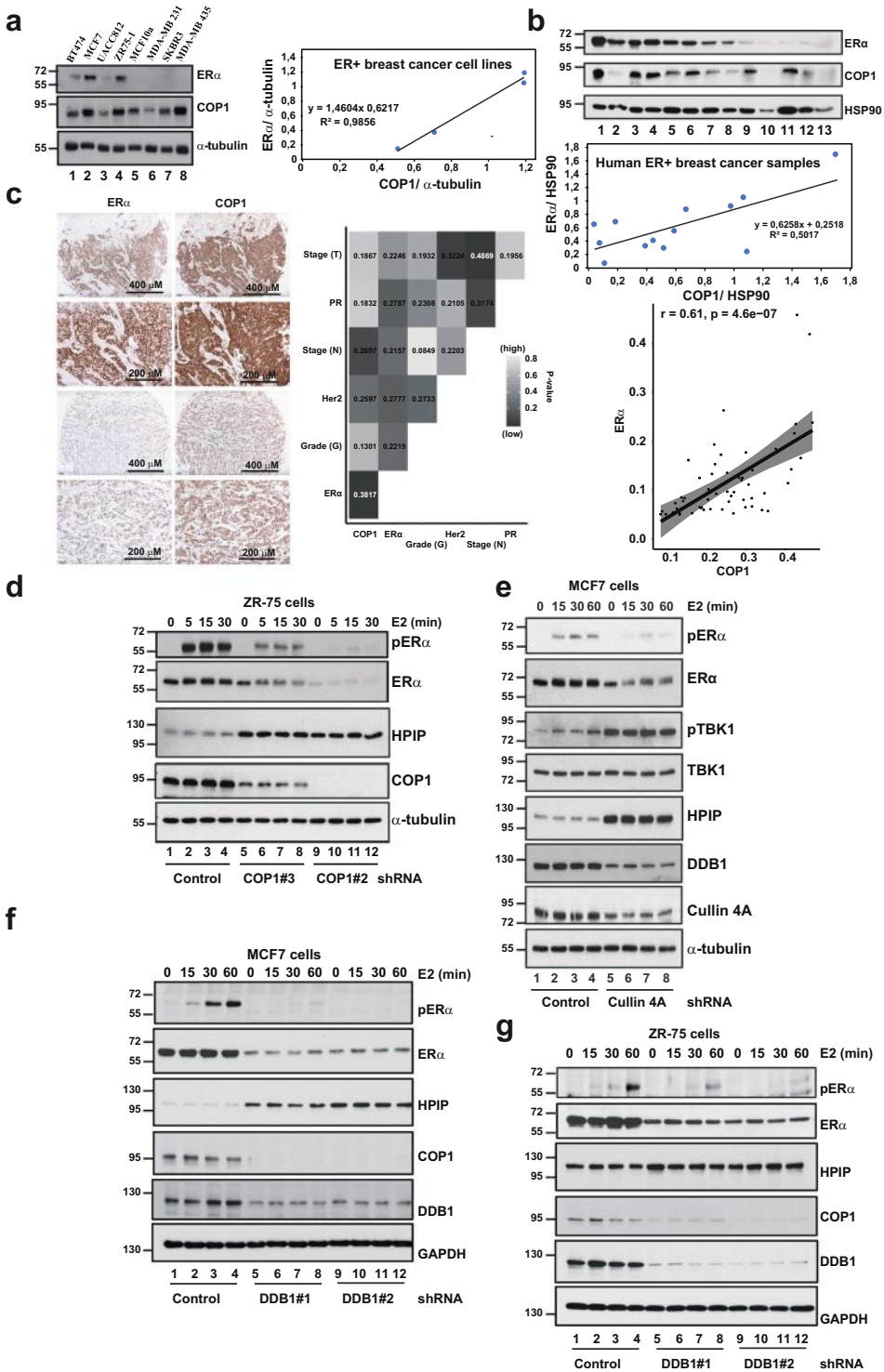

Fig. 3 COP1 promotes ERα expression in breast cancer. a and **b** COP1 and ERα protein levels are positively correlated in breast cancer-derived cell lines **(a)** and in clinical cases of breast cancer **(b)**. COP1 and ERα levels were assessed in the indicated cell lines **(a)** or in clinical cases of breast cancer **(b)** by WB. **c** ERα and COP1 protein levels are positively correlated in clinical cases of breast cancer. Immunohistochemical (IHC) evaluation of COP1 and ERα expression in 57 cases of human ER^{+} breast cancer was carried out. On the left, representative pictures of ERα and COP1 stainings for clinical cases showing high or weak levels of both proteins (upper and lower panels, respectively). On the right, correlation of ERα and COP1 staining intensities using categorial staining intensities graded from 0/weak to 3/strong in relation to clinical characteristics. The labels represent Cramer's V contingency coefficient, where values above 0.25 indicate a strong association. The color code of the squares shows significant values of the calculated chi-square tests, where darker colors indicate smaller *p* values. **d** COP1 deficiency in ZR-75 cells disrupts ERα signaling but enhances HPIP protein levels. Control and COP1-depleted ZR-75 cells were treated or not with E2 (10 nM) for the indicated periods of time and the resulting extracts were subjected to WB analyses using the indicated antibodies. **e-g** DDB1 and Cullin 4A promotes ERα signaling. Control and Cullin 4A-depleted MCF7 **(e)**, control and DDB1-depleted MCF7 cells **(f)** or control and DDB1-depleted ZR-75 cells **(g)** were treated or not with E2 (10 nM) for the indicated periods of time and the resulting extracts were subjected to WB analyses using the indicated antibodies.

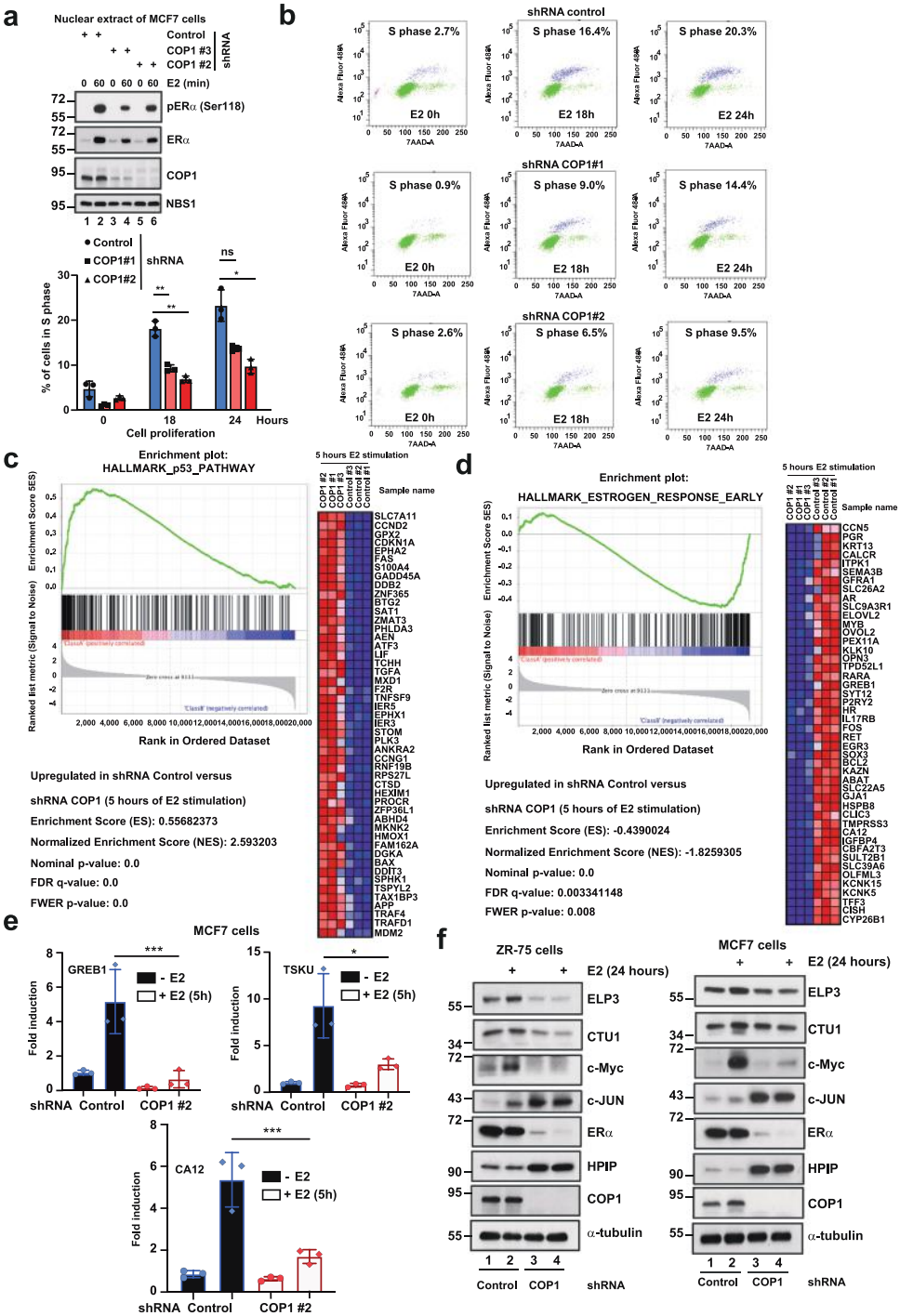

Fig. 4 The induction of ERα target genes by estrogens rely on COP1. a Decreased nuclear levels of both unphosphorylated and phosphorylated ERα levels upon COP1 deficiency in MCF7 cells. On the top, nuclear extracts from control and COP1-depleted MCF7 cells subjected to E2 stimulation (10 nM) or not were used for WB analyses using the indicated antibodies. The anti-NBS1 western blot was used for normalization purposes. **b** Cell proliferation induced by estrogens relies on COP1. Control and COP1-depleted MCF7 cells were treated or not with E2 (10 nM) for 18 or 24 hours and FACS analyses were conducted to quantify the percentage of cells in S phase. Representative FACS analyses are illustrated on the right. The percentage of cells in S phase was quantified in all experimental conditions (see the histogram at the bottom). Data from three independent experiments were plotted (means ± SD) (Two-way ANOVA test, $***P < 0.001$, $**P < 0.01$, $*P < 0.05$). **c** and **d** Enrichment of candidates linked to p53- and ERα-dependent gene transcription upon COP1 deficiency in MCF7 cells, as evidenced by GSEA analyses (**c** and **d**, respectively). FDR = False Discovery Rate. FWER = FamilyWise-Error Rate. **e** COP1 deficiency impairs the induction of ERα target genes upon stimulation by estrogens (5 hours). mRNA levels of the indicated genes were quantified by Real-Time PCR experiments in the indicated experimental conditions. mRNA levels in control and unstimulated cells was set to 1 and levels in other conditions were relative to that after normalization with β-actin. Data from two independent experiments performed in triplicates (means ± SD) (One-way ANOVA test, $***P \leq 0.001$, $*P < 0.05$) are shown. **f** COP1 controls the induction of multiple ERα target genes upon stimulation by estrogens in breast cancer cells. ZR-75 or MCF7 cells were treated or not with E2 (10 nM) for 24 hours and the resulting cell extracts were subjected to WB analyses.

COP1 deficiency in MCF7 cells (Supplementary Fig. 4a). ELP3 and CTU1, two tRNA-modifying enzymes recently defined as ERα target genes [24], were not properly induced by estrogens in both MCF7 and ZR75 cells in which the COP1 substrate c-Jun was stabilized, as expected (Fig. 4f). This lack of estrogens-dependent induction also applied to c-Myc, another ERα target gene (Fig. 4f). Importantly, DDB1 deficiency also impaired the induction of GREB1 by estrogens in both MCF7 and ZR-75 cells (Supplementary Fig. 4b). The expression of some candidates not regulated by estrogens was also deregulated upon COP1 deficiency in MCF7 cells. Indeed, mRNA levels of the Wnt target gene RUNX2-1, PMAIP1 and the COP1-interacting candidate TRIB1 were increased in COP1-depleted versus control MCF7 cells while ANXA6 levels were decreased upon COP1 deficiency (Supplementary Fig. 5a–c). Therefore, the ERα-dependent gene signature relies on the COP1 E3 ligase complex.

Stabilized c-Jun upon COP1 deficiency contributes to decreased ERα levels

COP1 deficiency in MCF7 cells results in decreased ERα mRNA levels, suggesting a defective transcription (Fig. 5a). The recruitment of RNA polymerase II on promoter B, which is one of the 7 described promoters of *ERα* gene [7], as well as at the transcription start was defective in COP1-depleted MCF7 cells (Fig. 5b). As COP1 deficiency prevents c-Jun degradation [19, 22] and because c-Jun appears to repress ERα transcription [14], we next explored whether decreased ERα expression seen upon COP1 deficiency results at least from c-Jun protein accumulation. Several AP-1 binding sites upstream the transcription start were identified on the *ERα* promoter (Fig. 5c). c-Jun recruitment on most of these AP-1 sites was enhanced upon COP1 deficiency (Fig. 5c). Moreover, c-Jun overexpression in MCF7 cells decreased ERα expression in a dose-dependent manner (Fig. 5d). The depletion of c-Jun in COP1-depleted MCF7 cells also partially restored ERα expression when compared to COP1 deficient cells (Fig. 5e). Finally, c-Jun and ERα levels were inversely correlated in breast cancer-derived cell lines, further supporting the hypothesis that c-Jun is a negative regulator of ERα expression (Fig. 5f). Therefore, COP1 promotes ERα expression, at least through c-Jun degradation.

Metabolic reprogramming by estrogens relies on COP1

Estrogens trigger metabolic reprograming in breast cancer cells, as reflected by enhanced aerobic glycolysis (i.e. increased glucose consumption and lactate production) and glutamate synthesis [25–27]. To further support the notion that COP1 mediates the biological effects of estrogens, we established the metabolomic signature of control and COP1-depleted cells treated or not with estrogens. MCF7 cells were selected given their strong metabolic response to estrogens [28]. Both glucose consumption and lactate production through aerobic glycolysis were enhanced by estrogens in control cells (Fig. 6a). A defective glycolysis was observed upon COP1 deficiency, as evidenced by both increased glucose and decreased lactate levels (Fig. 6a). Therefore, the metabolic reprogramming triggered by estrogens requires COP1 in these cells. Unexpectedly, our RNA-Seq experiments revealed that several candidates linked to glycolysis were actually up rather than downregulated upon COP1 deficiency (Fig. 6b–d). Indeed, mRNA levels of both LDHA and HK2 were increased in COP1-depleted MCF7 cells (Fig. 6d), which suggests a compensatory mechanism seen in cells that cannot execute glycolysis efficiently. However, both HK2 and LDHA protein levels were decreased upon COP1 deficiency, which further supports a defective glycolysis in these cells (Fig. 6e). SOX9 levels were severely increased upon COP1 deficiency in both MCF7 and T47D cells (Fig. 6b and Supplementary Fig. 6a, respectively). However, this conclusion did not apply to MDA-MB-231 cells (Supplementary Fig. 6a). Interestingly, SOX9 mRNA and protein levels were induced in MCF7 but not in MDA-MB-231 cells treated with 2-deoxy-D-glucose (2DG) or with 3-bromopyruvate (3BP), two glycolytic inhibitors (Supplementary Fig. 6b to 6e, respectively). FOXO3a, which induces SOX9 transcription in chondrocytes [29], was also induced by 2DG in MCF7 cells (Supplementary Fig. 6d). Therefore, breast cancer cells which fail to undergo glycolysis, a feature of COP1 deficiency or upon treatment with 2DG or with 3BP, enhances SOX9 expression.

To further address the link between COP1 and mitochondria activity, we next explored whether COP1 regulates mitochondrial oxidative phosphorylation based on the oxygen consumption rate (OCR), a measure of electron transport chain activity. Maximal and basal OCR were significantly decreased in untreated or estrogens-stimulated cells lacking COP1 (Fig. 6f). The spare OCR capacity was also decreased upon COP1 deficiency (Fig. 6f). Therefore, COP1 deficiency altered all major OCR compartments. Interestingly, glycolysis, assessed through measurement of the extra acidification rate (ECAR) was also defective upon COP1 deficiency (Fig. 6f). Here again, the basal, maximal and spare OCR were all defective in cells lacking COP1. Therefore, COP1 expression is required for mitochondrial functions in breast cancer cells.

COP1 deficiency triggers EMT through an ERα-independent pathway

The loss of an ERα-dependent transcriptional signature was not the only mechanism by which COP1 regulates breast cancer development. Indeed, we also highlighted a transcriptional signature of cells undergoing EMT upon COP1 deficiency (Fig. 7a). Beside elevated SOX9 protein levels seen in COP1-depleted MCF7 cells (Fig. 7b), levels of CEMIP, a positive regulator of EMT [30], were increased upon COP1 deficiency in MCF7 cells (Fig. 7b). Moreover, levels of the epithelial marker E-Cadherin decreased in COP1-depleted MCF7 cells, which reflects cells undergoing EMT (Fig. 7b). To assess whether this conclusion applies to another epithelial cell line, we depleted COP1 in MCF10A cells and observed that E-Cadherin levels also decreased, similarly to what we saw in MCF7 cells (Fig. 7b). Moreover, levels of the mesenchymal marker Vimentin increased upon COP1 deficiency in MCF10A cells (Fig. 7b). COP1-depleted cells also lost the typical localization of both E-Cadherin and ZO-1 in cytoplasmic membranes (Fig. 7c). mRNA levels of both positive regulators of EMT and Wnt target genes (CEMIP, EPHB6, AXIN2-1, WNT5A) as well as FAS were increased in COP1-depleted MCF7 cells (Fig. 7d). Therefore, COP1 deficiency triggers EMT in breast cancer cells. Consistently, invasive PyMT cells generated from PyMT mice and lacking COP1 expression showed enhanced migration abilities, as judged by a Boyden chamber assay (Fig. 7e). This enhanced migrating ability of COP1-depleted cells was also confirmed using an invasiveness assay carried out with mammospheres generated with control or COP1-depleted PyMT cells cultured in a Collagen I matrix. Indeed, the number of protrusions, which reflects cell migration, was increased upon COP1 deficiency (Fig. 7f). PyMT cells lacking COP1 also showed elevated HPIP levels as well as enhanced AKT activation by estrogens (Supplementary Fig. 7a). Consistently, Greb1 induction by estrogens in these cells was also defective upon COP1 deficiency (Supplementary Fig. 7b). Therefore, our conclusions apply to a variety of breast cancer cells.

As cells undergoing EMT show features of cancer stem cells [31], we quantified the pool of $CD24^{+}/CD44^{+}$ cancer stem cells by FACS analyses in both control and COP1-depleted MCF7 cells. The pool of $CD24^{+}/CD44^{+}$ cells was enhanced upon COP1 deficiency (Fig. 8a). Consistently, CD44 protein levels were also increased in COP1-depleted MCF7 cells (Fig. 8b). COP1-depleted cells generated loose mammospheres, which is a feature of cancer cells which underwent EMT (like MDA-MB-231 cells which derived from a triple negative breast cancer) (Fig. 8c). Therefore, the loss of COP1 triggers EMT in breast cancer cells.

To assess whether COP1 prevents EMT through an ERα-dependent pathway, we depleted ERα in MCF7 and explored the consequences on both epithelial and mesenchymal markers. SOX9 protein and

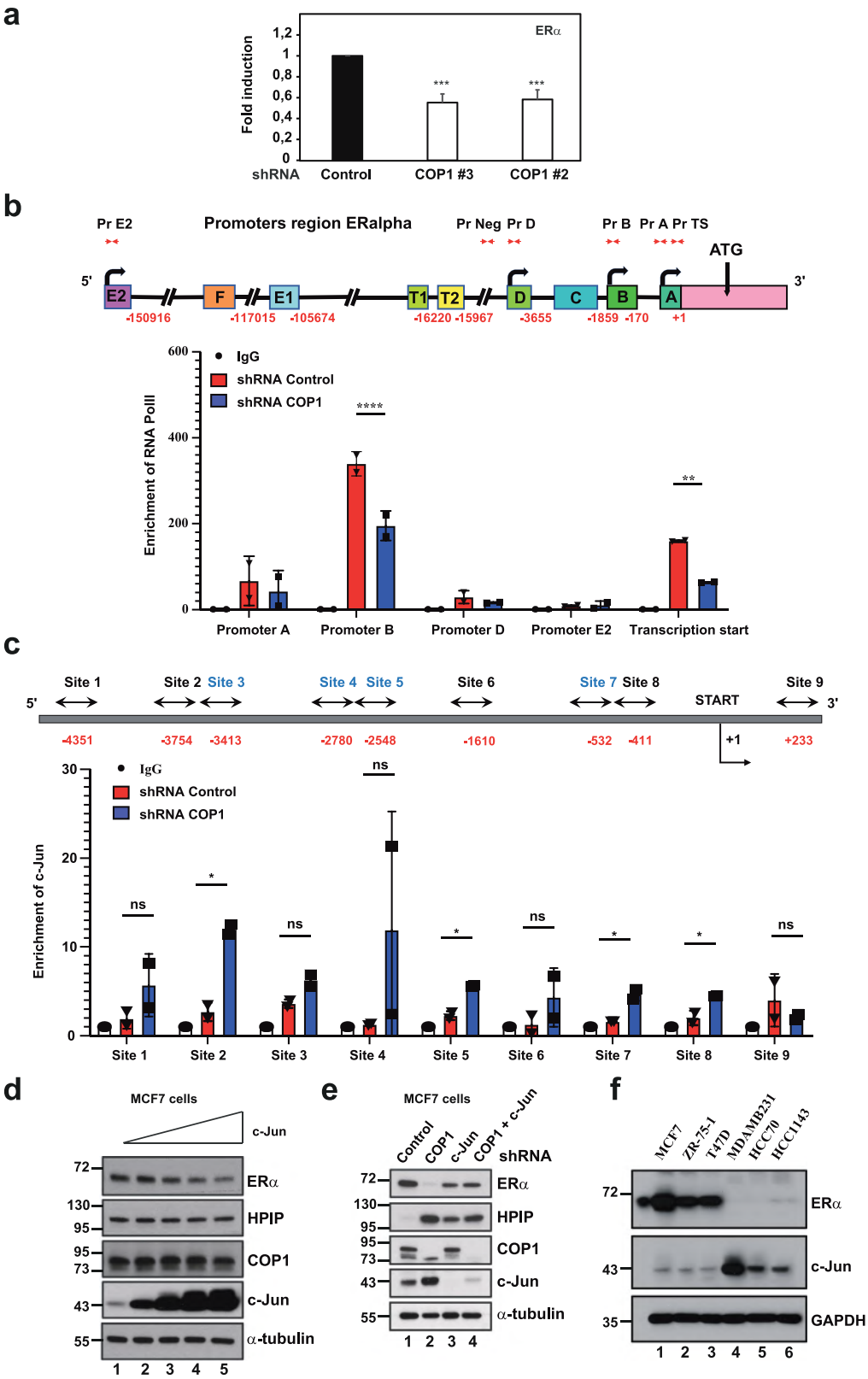

mRNA levels were also increased upon ERα deficiency in MCF7 cells (Supplementary Fig. 8a and b, respectively). Whereas FAS mRNA levels also increased upon ERα deficiency, Wnt target genes (WNT5A, EPHB6 and AXIN2-1) remained unchanged (Supplementary Fig. 8b), as were both CEMIP and E-cadherin protein levels (Supplementary Fig. 8a). Consistently, the pool of $CD24^{+}/CD44^{+}$ cancer stem cells was not amplified in ERα-depleted MCF7 cells (Supplementary Fig. 8c). Therefore, ERα deficiency does not trigger EMT in MCF7 cells, which implies that COP1 prevents EMT through an ERα-independent pathway.

Fig. 5 c-Jun is a negative regulator of ERα expression. a Decreased ERα mRNA levels upon COP1 deficiency. ERα mRNA levels was quantified by Real-Time PCR experiments in the indicated experimental conditions. mRNA levels of ERα in MCF7 cells infected with control shRNAs were set to 1 and levels in other experimental conditions were relative to that after normalization with glyceraldehyde-3-phosphate dehydrogenase (GAPDH). The figure shows the data from three independent experiments performed on two distinct infections (means ± SD) (Student's *t* test, ***$P < 0.001$). **b** Defective RNA Polymerase II recruitment on *ERα* promoter upon COP1 deficiency. On the top, schematic illustration of *ERα* promoters, using the suggested nomenclature [7]. The location of all primers used in ChIP assays is depicted by red arrows. Histogram shows RNA polymerase II recruitment on the indicated *ERα* promoters in control and COP1-depleted MCF7 cells. The anti-IgG antibody was used as negative control. Results of two independent experiments (means ± SD) (Two-way ANOVA *t* test, *$P < 0.05$, **$P < 0.01$) are shown. **c** Enhanced c-Jun recruitment on the *ERα* promoter upon COP1 deficiency. AP-1 binding sites were identified (Tfbind software) and ChIP assays using an anti-c-Jun antibody were carried out. Histogram shows c-Jun recruitment on indicated sites (the anti-IgG antibody was used as negative control). Results of two independent experiments (means ± SD) (Two-way ANOVA test, *$P < 0.05$, **$P < 0.01$, ***$P < 0.001$) are shown. **d** c-Jun overexpression decreases ERα expression in breast cancer cells. MCF7 cells were transfected with increasing amounts of a c-Jun-expressing plasmid and WB analyses were carried out with the resulting extracts. **e** Depletion of c-Jun in COP1-depleted cells partially restores ERα levels. MCF7 cells were infected with the indicated shRNA lentiviral constructs and the resulting extracts were subjected to WB analyses using the indicated antibodies. **f** c-Jun and ERα levels are inversely correlated in breast cancer-derived cell lines. WB analyses were carried out with extracts from the indicated cell lines.

COP1 deficiency promotes Tamoxifen resistance

In contrast to triple negative breast cancers which, by definition, lost ERα expression, patients suffering from ERα$^+$ breast cancers can benefit from a treatment with Tamoxifen, a non-steroidal, anti-estrogen drug. As the loss of ERα expression is one mechanism underlying Tamoxifen resistance in breast cancer [32] and given the fact that COP1 promotes ERα expression, we assessed whether COP1-depleted MCF7 cells are resistant to Tamoxifen. In agreement with our GSEA analyses, most COP1-depleted cells underwent cell death but some of them escaped from this process and were treated with Tamoxifen in parallel with control MCF7 cells. Tamoxifen dramatically interfered with colony formation of control but not COP1-depleted MCF7 cells (Fig. 9a). COP1-depleted cells actually generated more colonies when treated with Tamoxifen, which confirms their insensitivity to this drug (Fig. 9a). Consistently, COP1-depleted MCF7 cells were largely insensitive to Tamoxifen as the number of viable cells did not change overtime (Fig. 9b). Indeed, cell viability of control but not COP1-depleted cells MCF7 significantly decreased upon Tamoxifen treatment (Fig. 9b).

Protective autophagy, a strategy of cellular self-degradation and cell survival in response to apoptotic, pro-cell death signals such as chemotherapy, plays a role in Tamoxifen resistance [33, 34]. Interestingly, COP1 deficiency enhanced the percentage of MCF7 cells showing autophagosome formation upon Tamoxifen treatment, as evidenced by both anti-LC3 and -p62 immunofluorescence analyses (Fig. 9c). Indeed, Tamoxifen more robustly triggered autophagy (as assessed by LC3 cleavage) in COP1-depleted than in control MCF7 cells (Fig. 9d). COP1 deficiency also interfered with Rb phosphorylation seen upon Tamoxifen treatment (Fig. 9d). Of note, COP1 deficiency in unstimulated cells did not trigger autophagy as LC3 cleavage remained similar in both control and COP1-depleted MCF7 cells (Fig. 9d). Therefore, COP1 deficiency is linked to Tamoxifen resistance, at least through protective autophagy.

To further explore how COP1 deficiency promotes autophagy, we addressed AMPK activation in MCF7 cells lacking or not COP1 expression, given the key role of AMPK in autophagy [35]. AMPK activity was strongly enhanced in cells lacking COP1 and this status was also observed upon E2 stimulation (Fig. 9e). Moreover, COP1 negatively regulates AMPK activation through a HPIP-independent pathway as AMPK phosphorylation remained elevated in cells lacking both HPIP and COP1 (Fig. 9e). AMPK promotes autophagy through the phosphorylation of multiple substrates including ULK [36, 37]. Consistently, COP1 deficiency potentiated AMPK- but not mTOR-dependent ULK phosphorylation as ULK phosphorylation on serine 555 but not on serine 757 was elevated in cells lacking COP1 (Fig. 9f). Therefore, COP1 deficiency promotes protective autophagy, at least through AMPK activation. As COP1 deficiency impairs ERα levels, we next explored whether ERα deficiency also triggered autophagy. Both wild type and p53-depleted MCF7 cells lacking ERα showed more autophagy upon Tamoxifen treatment (Fig. 9g). Therefore, ERα and COP1 deficiencies share similar consequences on Tamoxifen-mediated autophagy.

DISCUSSION

We show here that the E3 ligase COP1 has a dual role in breast cancer, which results from its capacity to target multiple substrates. Indeed, COP1 promotes ERα signaling with consequences on estrogens-dependent gene transcription, proliferation, and metabolic reprogramming. As such, COP1 acts as an oncogene. Importantly, COP1 also acts as a tumor suppressor gene by limiting estrogens-dependent AKT activation and by preventing both EMT and enhanced SOX9 expression. The oncogenic role of COP1 may be predominant in ERα$^+$ breast cancers while its tumor suppressive role could be predominant once ERα is lost (Fig. 10).

The search for new E3 ligases targeting HPIP led to the identification of COP1. In contrast to MDM2, another E3 ligase for HPIP, COP1 promotes rather than inhibits ERα expression and signaling [17]. Indeed, while MDM2 deficiency causes HPIP stabilization and consequently enhanced ERα protein levels, COP1 deficiency impairs ERα expression, at least through c-Jun stabilization. Therefore, the differential effect of COP1 and MDM2 on ERα expression may result from the fact that c-Jun is targeted for degradation by COP1 but not by MDM2.

We show that COP1 deficiency causes c-Jun stabilization in breast cancer cells, as also previously seen in mice [19, 22]. Therefore, COP1 promotes c-Jun degradation in both normal and cancer cells. Consistently, COP1 deficiency is linked to a robust AP-1-dependent signature in breast cancer cells, as demonstrated by our GSEA analyses. Thus, stabilized c-Jun appears to be transcriptionally active, presumably as a dimer with other AP-1 members, in COP1-depleted cells. As a result, ERα, a gene known to be repressed by c-Jun [13, 14], is downregulated upon COP1 deficiency. This finding is clinically relevant as ERα and c-Jun levels are inversely correlated in cases of human breast cancers. Whereas it is now well established that c-Jun is a target of COP1 in multiple cell types, the link between COP1 deficiency and p53 activation appears to be cell type-dependent. Indeed, we show that COP1 deficiency is linked to a p53-dependent apoptotic signature in breast cancer cells. This finding supports the initial observation that p53 is targeted by COP1 in cancer cells, as confirmed in glioma cells [23, 38]. However, despite the fact that a p53-dependent gene signature was observed upon COP1 deficiency in MCF7 cells, we did not see any dramatic increase of p53 protein levels upon COP1 deficiency, no matter which shRNA was used to deplete COP1. Because p53 protein levels are not changed in mice

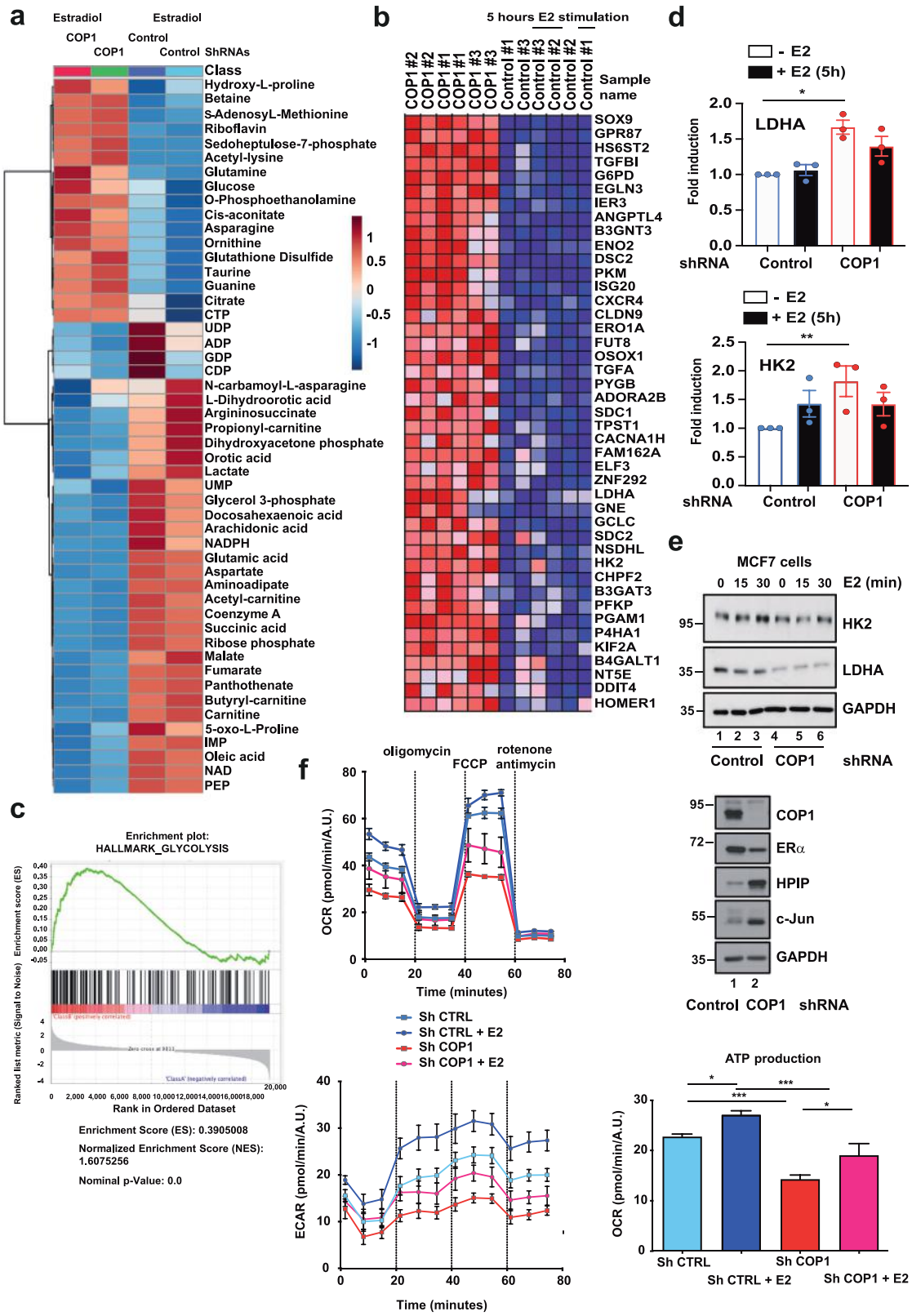

in which COP1 is deficient, it remains unclear how COP1 limits p53 pro-apoptotic function in breast cancer but not in normal cells.

Metabolic reprogramming by estrogens, including aerobic glycolysis, critically relies on COP1 as its deficiency blocks the production of lactate from glucose. In the same time, our GSEA analyses highlighted a glycolytic signature upon COP1 deficiency, as evidenced by enhanced mRNA levels of key enzymes such as HK2. This paradoxical observation may reflect a compensatory mechanism as protein levels of HK2 and LDHA are decreases upon COP1 deficiency. Our functional studies actually support the fact that COP1

Fig. 6 Metabolic reprogramming by estrogens requires COP1. a COP1 promotes metabolic reprogramming by estrogens in breast cancer cells. The metabolomic profile was established in control versus COP1-depleted MCF7 cells treated or not with E2 (10 nM) for 24 hours. Data are presented as heatmap visualization and hierarchical clustering analysis of top 50 compounds (Student *t* test, $P < 0.05$). Rows: metabolites; columns: samples; color key indicates metabolite expression value (blue: lowest; red: highest). Data with triplicates are presented. **b** and **c** Upregulation of mRNA levels of candidates involved in glycolysis upon COP1 deficiency in breast cancer cells. A heatmap was generated with RNASeq data obtained from control versus COP1-depleted MCF7 cells treated or not with E2 for 5 hours. Genes upregulated in COP1-depleted cells are depicted as red squares **(b)**. GSEA analyses carried out with RNASeq data obtained with RNAs from control versus COP1-depleted MCF7 cells are illustrated **(c)**. **d** Enzymes involved in glycolysis are upregulated at the mRNA level upon COP1 deficiency in breast cancer cells, as evidenced by Real-Time PCRs. Cells were untreated or stimulated with E2 (10 nM) for the indicated time. mRNA levels of LDHA and HK2 in unstimulated MCF7 cells infected with control shRNA were set to 1 and levels in other experimental conditions were relative to that after normalization with glyceraldehyde-3-phosphate dehydrogenase (GAPDH). The figure shows the data from three independent experiments performed on two distinct infections (means ± SD) (One-way ANOVA test, $*P < 0.05$, $**P < 0.01$). **e** COP1 deficiency impairs LDHA and HK2 protein levels upon estrogens stimulation. Control or COP1-depleted MCF7 cells were treated or not with E2 (10 nM) for the indicated periods of time and the resulting cell extracts were subjected to WB analyses. **f** COP1 deficiency in breast cancer cells impairs glycolysis and oxidative phosphorylation. On the right, extracts from control and COP1-depleted cells were subjected to WB analyses. Basal, maximal and spare oxygen consumption rate (OCR) as well as basal and maximal extracellular acidification rate (ECAR) were measured with extracts from control and COP1-depleted MCF7 cells treated or not with E2 (10 nM). Data were normalized according to cell numbers (see methods for details on statistics). All seahorse experiments were performed as independent triplicates.

promotes both glycolysis and oxidative phosphorylation in breast cancer cells as basal and maximal OCR as well as ECAR were defective upon COP1 deficiency. Moreover, COP1 supports glycolysis through an ERα-dependent pathway. COP1 or ERα depletion in MCF7 cells leads to higher SOX9 levels. Consistently, the pharmacological inhibition of glycolysis also upregulates SOX9 expression. Enhanced SOX9 expression may occur through a FOXO3-dependent pathway, as already demonstrated in periosteal cells [29].

COP1 deficiency leads to the expansion of the pool of cancer stem cells in MCF7 cells, which may reflect a key mechanism by which COP1 acts as a tumor suppressor gene. Such conclusion does not apply to ERα-depleted cells in which SOX9 expression was nevertheless increased. Therefore, SOX9 is not sufficient for the expansion of cancer stem cells seen upon COP1 deficiency. Preventing the expansion of cancer stem cells is not the only mechanism by which COP1 acts as a tumor suppressor gene. Indeed, we also show that COP1 prevents EMT through an ERα-independent pathway in breast cancer cells. HPIP, which promotes EMT through AKT [39], is stabilized upon COP1 deficiency. It is likely that the accumulation of additional and unidentified COP1 substrates contributes to EMT seen upon COP1 deficiency. Likewise, our functional studies confirm that COP1 deficiency enhances the invasiveness of breast cancer cells which opens the possibility that COP1 deficiency may promote breast cancer metastasis.

MDM2 and COP1, two E3 ligases for HPIP, differentially regulates ERα expression, As a result, while MDM2 deficiency sensitizes breast cancer cells to Tamoxifen through ERα stabilization [17], COP1 deficiency causes Tamoxifen resistance. These data suggest that two E3 ligases having at least one common substrate involved in ERα signaling such as HPIP can differentially regulate Tamoxifen resistance because of their distinct networks of substrates. Our data indicate that the loss or the decreased expression of COP1, which is seen in TNBCs [40], contributes to Tamoxifen resistance. Rb phosphorylation on Ser 807/811 is a feature of cells undergoing cell cycle progression [41]. COP1-depleted MCF7 cells, which underwent EMT, do not proliferate as much as control cells and fails to phosphorylate Rb upon Tamoxifen treatment. It is known that EMT progression requires cycle arrest. Therefore, the lack of response of COP1-depleted cells to Tamoxifen supports the fact that EMT confers resistance to targeted therapies [42]. Mechanisms by which COP1 deficiency promotes Tamoxifen includes protective autophagy, at least through AMPK activation. Although it remains to be demonstrated how COP1-depleted breast cancer cells promote AMPK activation, ATP production is defective in these cells and an altered AMP/ATP ratio triggers AMPK activation [43]. Therefore, Tamoxifen resistance seen with COP1-depleted cells may result from a defective metabolic reprogramming. In any case, this process results at least from the loss of ERα expression in COP1-depleted cells as protective autophagy was also seen upon ERα deficiency.

Mouse models of breast cancer in which *COP1* is genetically deleted are required to define whether COP1 acts as an oncogene or as a tumor suppressor gene in vivo. The genetic inactivation of *COP1* in mouse prostate epithelia cells enhances cell proliferation and causes early prostate intraepithelial neoplasia, at least through the accumulation of some ETS transcription factors [20]. Whether this conclusion applies to mammary malignancies remains to be experimentally addressed. Our report indicates that the function of COP1 in breast cancer development and progression may critically relies on ERα status.

MATERIALS AND METHODS

Cell culture, biological reagents, and treatments

HEK293 and Lenti-X 293T cells were maintained in culture as described [44] whereas ZR-75, MCF7, T47D, BT474, SKBR3, MDA-MB-435, and MDA-MB-231 cells were cultured in DMEM supplemented with 10% fetal calf serum and antibiotics, as were p53-deficient MCF7 cells. HCC70, HCC1143 cells were cultured in DMEM supplemented with 20% fetal calf serum and antibiotics. UACC812 cells were cultured in DMEM/F12 with 20% fetal calf serum and antibiotics. PyMT cells (a gift from Arnaud Blomme, Laboratory of Cancer Signaling, University of Liege, Liege, Belgium) were cultured in RPMI with 10% fetal calf serum and antibiotics. MCF10A cells were culture in Mammary Epithelial Cell Growth Basal Medium (CC-3151, Lonza, Basel, Switzerland) and supplemented with 100 ng/ml cholera toxin (C8052, Sigma-Aldrich) and mammary epithelial cell growth medium supplement mix (Promocell C-39115, Bioconnect Life Sciences). All cell lines were tested for Mycoplasma contaminations on a regular basis. For E2 treatments (10 nM), control, COP1- or p53-deficient MCF7 cells were first cultured for 72 hours with DMEM/F12 w/o phenol red supplemented with Charcoal/Dextran treated FBS (Hyclone/Fisher). For EGF treatments, cells were first serum starved for 24 hours. Breast adenocarcinomas samples were provided by the BioBank (CHU, Liege). All studies with those samples were approved by the Ethical Committee. 2-deoxy-D-glucose (2DG) and with 3BP were purchased from Sigma and from Toronto Research Chemicals, respectively. Tamoxifen was purchased from Sigma.

FLAG-HPIP, FLAG-HPIP S147A, FLAG-HPIPΔN60, -HPIPΔN150, and -HPIPΔN160 constructs were previously described [17, 45]. FLAG-HPIPΔC250, -ΔC300, -ΔC350, -ΔC400, -ΔC450, and -ΔC500 HPIP constructs were generated by PCR, using FLAG-HPIP as the template. FLAG HPIP K274R, K277R, and K293R were generated with the QuickChange Site-Directed Mutagenesis kit (Agilent Technologies, Santa Clara, CA, USA), using FLAG HPIP as the template. The COP1-Myc construct was generated by subcloning the COP1-coding sequence into the pCMV-N-Myc plasmid. HA-Ub and HDM2-Myc expression plasmids were previously described [17]. The Cullin 4A-Myc constructs was generated by subcloning the Cullin 4A coding sequence into the pCMV-Myc plasmid.

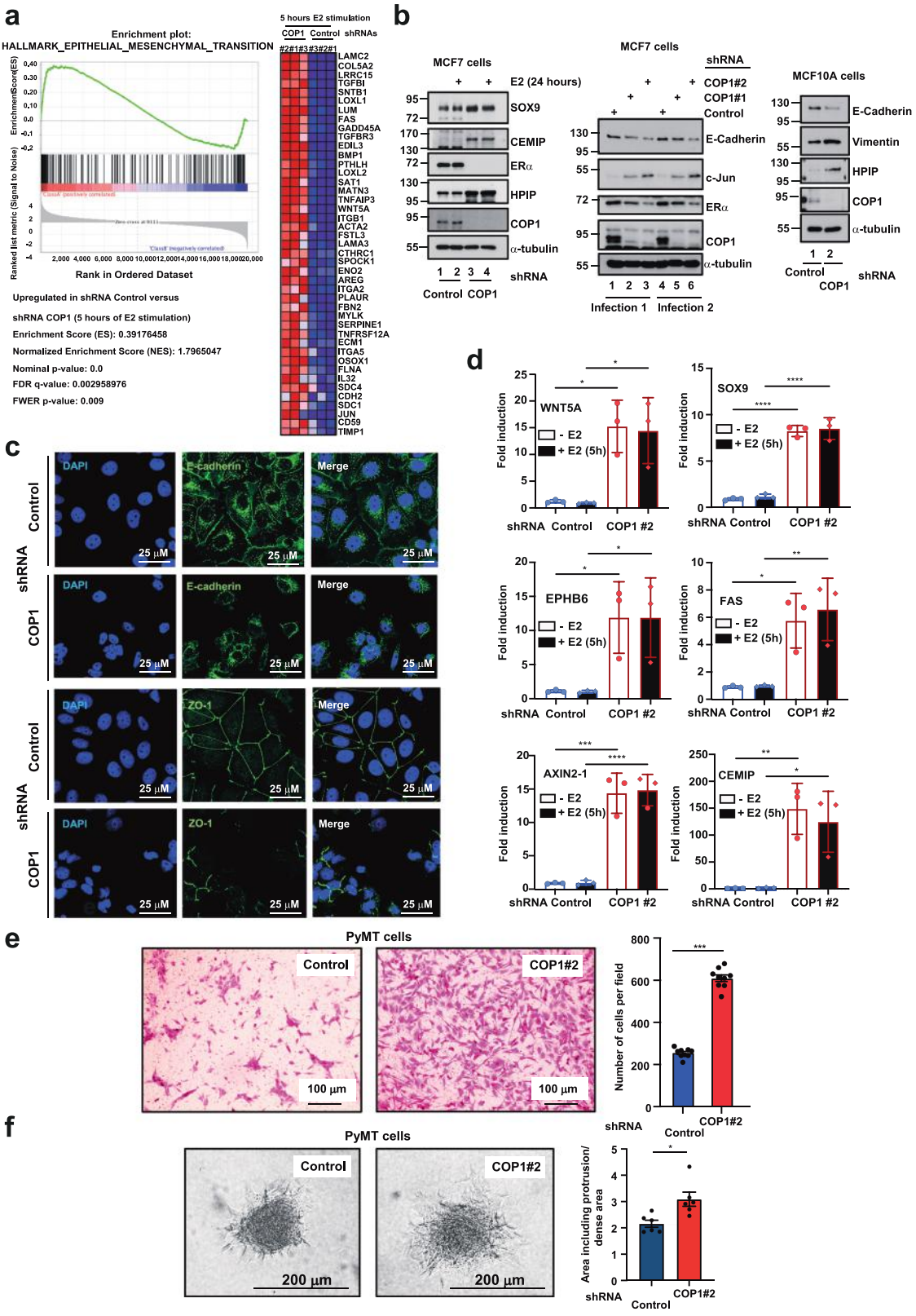

Cell lysis and western blot analyses

Cells were lysed in a buffer containing 50 mM/L Tris-HCl pH 8.0, sodium chloride 150 mM, sodium fluoride 50 mM, EDTA 2 mM, Nonidet P-40 1%, sodium deoxycholate 0.5%, SDS 0.1%, protease inhibitors, and phosphatase inhibitors. Human ERα-positive breast cancer tissue were lysed in 1% SDS buffer and homogenized with a plastic pestle. Tissue lysates were then boiled at 99 °C for minutes and centrifuged at 14,000 rpm for 10 minutes to obtain the supernatant. The supernatant was collected and the protein concentrations were measured using the Micro BCA™ protein assay kit. Western blots were carried out using antibodies listed in Supplementary Table 1. The quantification of key western blots using the Image J sofware is illustrated in Supplementary Figs. 9–13.

Fig. 7 COP1 expression prevents EMT. a COP1 deficiency is linked to an EMT transcriptional signature. GSEA analyses highlight an EMT signature in COP1-depleted MCF7 cells. Genes upregulated in COP1-depleted cells are depicted as red squares. **b** COP1 deficiency causes enhanced expression of mesenchymal markers and decreased E-Cadherin levels. Extracts from control or COP1-depleted MCF7 or MCF10A cells were subjected to WB analyses using the indicated antibodies. When relevant, cells were treated with E2 (10 nM) for the indicated period of time. **c** The localization of both E-Cadherin and ZO-1 at the cytoplasmic membrane is deregulated upon COP1 deficiency. Immunofluorescence analyses were conducted in both control and COP1-depleted MCF7 cells to assess the cellular localization of epithelial markers. **d** COP1 deficiency leads to enhanced mRNA levels of EMT positive regulators, Wnt target genes and FAS. Cells were treated or not with E2 (10 nM) for the indicated period of time. mRNA levels of candidates in untreated MCF7 cells infected with control shRNA were set to 1 and levels in other experimental conditions were relative to that after normalization with glyceraldehyde-3-phosphate dehydrogenase (GAPDH). The figure shows the data from three independent experiments performed on two distinct infections (means ± SD) (One-way ANOVA test, $*P < 0.05$, $**P < 0.01$, $***P < 0.001$, $****P < 0.0001$). **e** COP1 deficiency enhances cell migration. Control or COP1-depleted PyMT cells were subjected to a Boyden chamber assay to assess cell migration. Pictures of 3 random fields were taken for each chamber. The number of cells were calculated in each field using the ImageJ software (means ± SD) (Student's *t* test, $***P < 0.001$). **f** COP1 deficiency potentiates invasiveness. Mammospheres of control and COP1-depleted PymT cells were plated in collagen I matrix. Pictures were taken 24 hours after plating. Invasiveness was calculated using the ImageJ software. The total area of spheroids including protrusions was divided by the dense area of spheroids ($n = 6$) (means ± SD) (Student's *t* test, $*P < 0.05$).

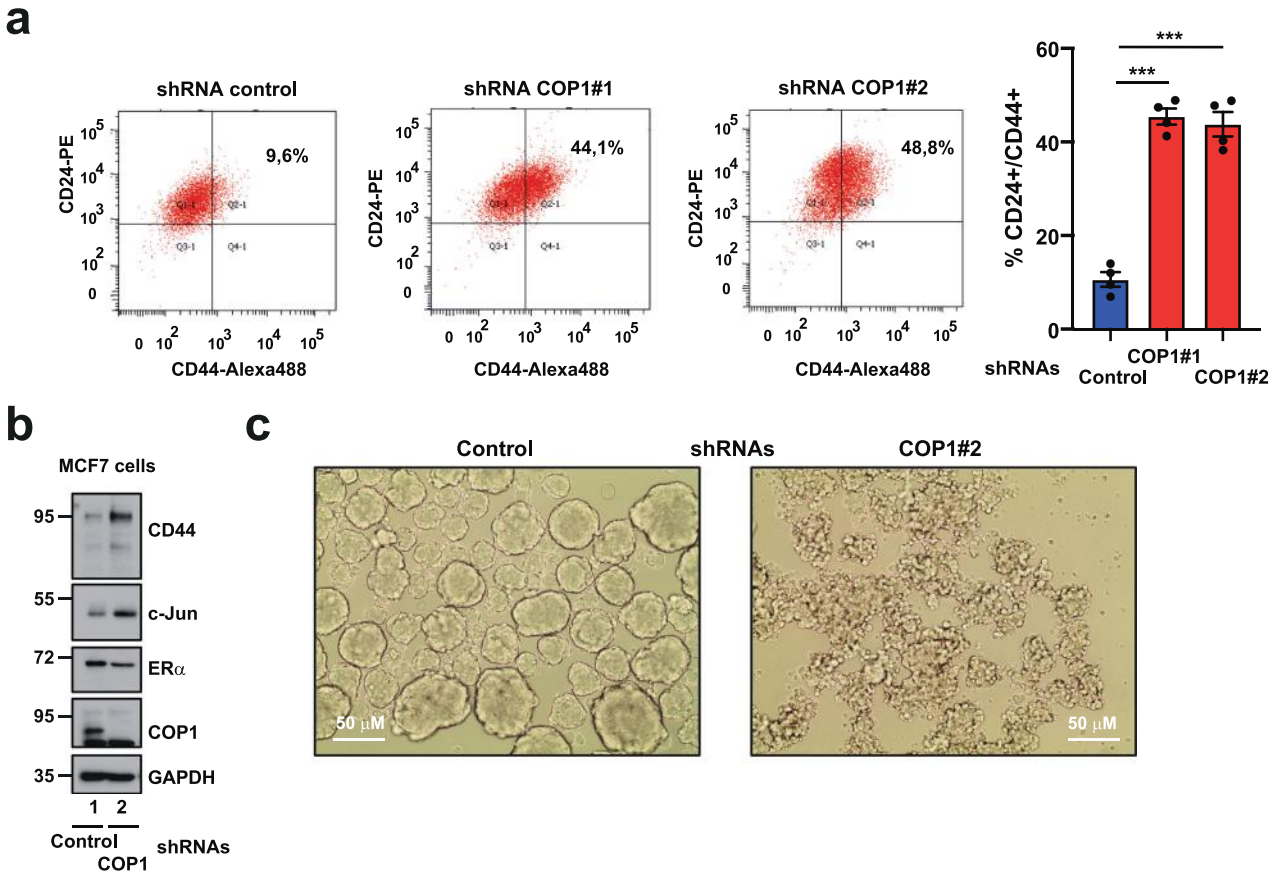

Fig. 8 COP1 negatively regulates the pool of cancer stem cells. a COP1 deficiency amplifies the pool of cancer stem cells. Control and COP1-depleted MCF7 cells were subjected to FACS analyses to quantify the pool of $CD24^+/CD44^+$ cells. The histogram shows data from two independent experiments performed in triplicates (means ± SD) (One-way ANOVA test, $*P < 0.001$). **b** COP1 deficiency enhances CD44 expression in breast cancer cells. Extracts from both control and COP1-depleted MCF7 cells were subjected to WB analyses using the indicated antibodies. **c** COP1 deficiency interferes with mammosphere formation. Control versus COP1-depleted cells were used to generate mammospheres using the appropriate experimental conditions (see methods for details).

Immunohistochemistry analyses

Immunohistochemical evaluation of COP1 and ERα expression was carried out using a commercially available Tissue microarray of human breast cancer (BC081120c, BioCat GmbH) in 57 cases of human ER^+ breast cancer. Antibodies were purchased from Abcam (COP1: ab56400; ERα: ab75635). All stainings were performed on a BOND MAX from Leica (Leica, Wetzlar, Germany) according to the manufacturer's protocol. For the purpose of quantification, the whole slide tissue microarrays were scanned on a NanoZoomer S360 digital slide scanner from Hamamatsu (Hamamatsu Photonics K.K.). Quantification was carried out by trained pathologists (Reinhard Büttner and Sebastian Klein) following a categorial grading system for strong positive (+++), positive (++), weak positive (+) and negative staining (−) intensities. Correlation of staining intensities and clinical characteristics was performed using the Cramer's V contingency coefficient, where values above 0.25 indicate a strong association.

Screening of the siRNA E3 ligase library

A Human E3 ligase library (G-005600, Dharmacon, Lafayette, CO, USA) was screened according to the protocol provided by the manufacturer, as previously described [17]. MCF7 cells were transfected in 96 wells with

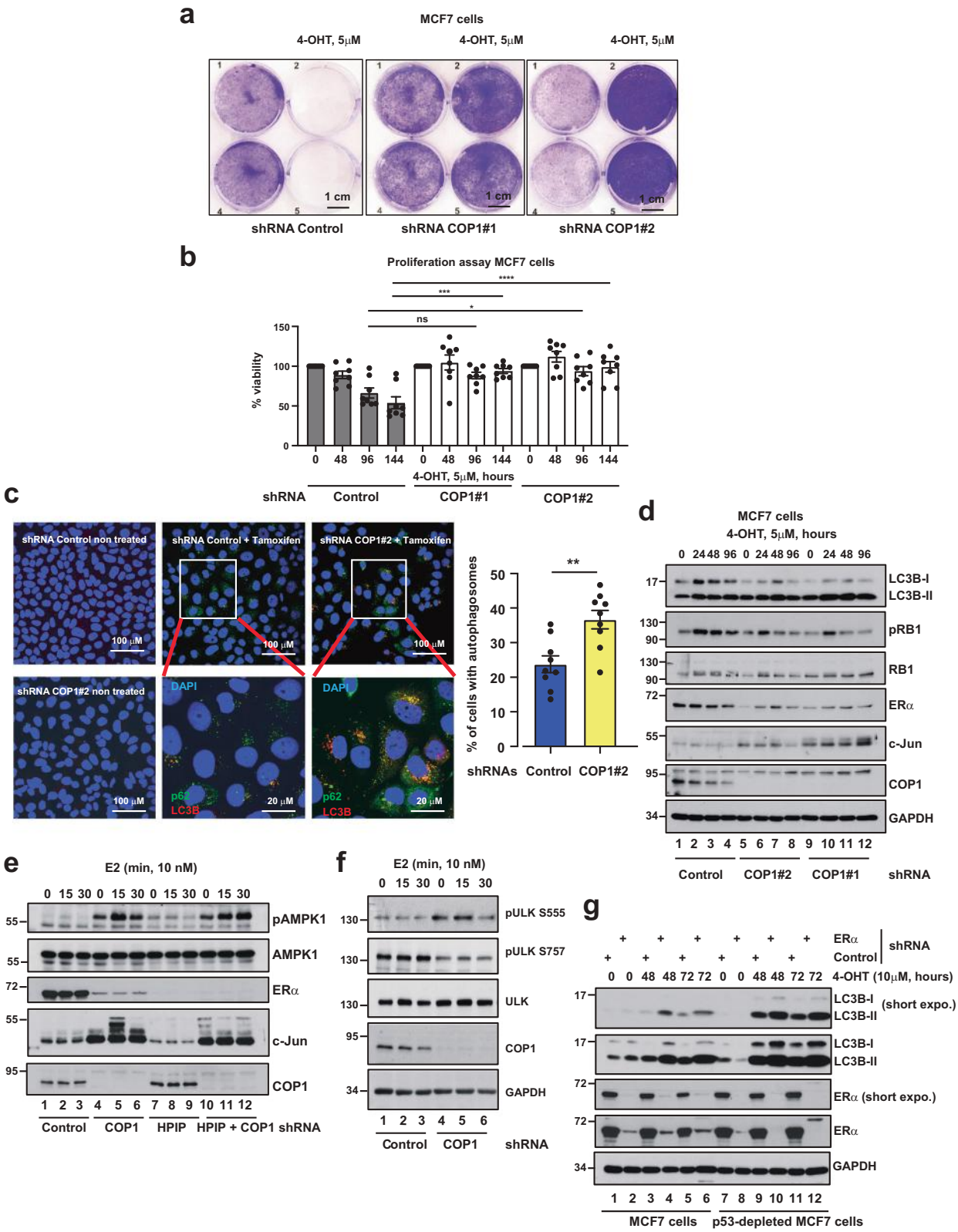

pool of distinct siRNAs targeting the same transcripts in duplicate using HiPerfect reagent (Qiagen). 48 hours after transfection, cells were harvested, lysed with 1% SDS buffer and HPIP, TBK1 and α-tubulin protein levels were assessed by Western Blot analysis. All signals were quantified by densitometry. The HPIP/α-tubulin ratio obtained in MCF7 transfected with the GFP siRNA was set to 1 and ratio obtained in other experimental conditions were expressed relative to that. Any candidate whose siRNA-mediated depletion gave a HPIP/α-tubulin ratio similar or higher to the one obtained in TBK1-depleted cells (positive control) was selected. A second screening performed with the selected siRNA sequences was subsequently carried out for confirmatory purposes. Datas from the second screening are shown.

Fig. 9 COP1 deficiency promotes Tamoxifen resistance. a COP1 deficiency promotes Tamoxifen resistance. Control and COP1-depleted cells treated or not with Tamoxifen were subjected to a colony formation assay. **b** COP1 deficiency prevents the decreased cell number of breast cancer cells treated with Tamoxifen. The number of control and COP1-depleted MCF7 cells treated or not with Tamoxifen (5 μM) was quantified. Cell viability in control and untreated MCF7 cells was set to 100% and values in other experimental conditions were related to that. The figure shows data from three independent experiments (means ± SD) (Two-way ANOVA test, $^{**}P < 0.01$). Cell viability in control and untreated MCF7 cells was set to 100% and values in other experimental conditions were related to that (means ± SD) (Two-way ANOVA test, $^{*}P < 0.05$, $^{**}P < 0.01$, $^{***}P < 0.001$). **c** COP1 deficiency causes enhanced autophagosome formation upon Tamoxifen treatment. Control and COP1-depleted MCF7 cells treated or not with Tamoxifen (5 μM for 24 hours) were subjected to anti-LC3 and p62 immunofluorescence analyses. The percentage of cells per field showing some autophagosomes was quantified in both control and COP1-depleted cells (means ± SD) (Student's *t* test, $^{**}P < 0.01$). 552 control and 555 COP1-depleted cells were counted on 9 distinct fields. **d** COP1 limits autophagy and promotes Rb phosphorylation upon Tamoxifen treatment. Extracts from control and COP1-depleted MCF7 cells treated or not with Tamoxifen for the indicated periods of time were subjected to WB analyses. **e** COP1 deficiency enhances E2-dependent AMPK activity through a HPIP-independent pathway. Control, COP1-, HPIP- or COP1 and HPIP-depleted MCF7 cells were treated or not with E2 for the indicated periods of time and the resulting cell extracts were subjected to WB analyses. **f** COP1 deficiency enhances AMPK- but not mTORC1-dependent ULK phosphorylation. Control or COP1-depleted MCF7 cells were treated or not with E2 for the indicated periods of time and the resulting cell extracts were subjected to WB analyses. **g** ERα deficiency enhances autophagy triggered by Tamoxifen. Control or p53-depleted MCF7 cells were infected with a control shRNA or with a shRNA construct targeting ERα. Cells were subsequently treated with 4-OH for the indicated periods of time and the resulting cell extracts were subjected to WB analyses.

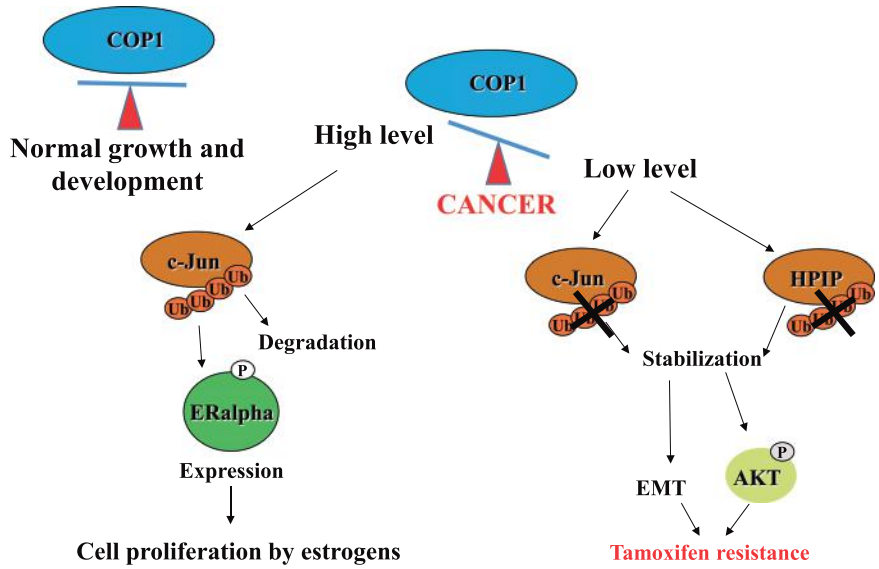

Fig. 10 A dual role for COP1 expression in breast cancer. High COP1 expression is detected in $ER\alpha^{+}$ breast cancer. COP1 promotes the degradative polyubiquitination of c-Jun, a repressor of ERα transcription. As a result, ERα transcription is enhanced and cell proliferation induced by estrogens can occur. Therefore, COP1 positively regulates tumor development in these tumors. In TNBC cases, COP1 expression is lost or decreased, which negatively regulates c-Jun degradative polyubiquitination. As a result, c-Jun is stabilized. As COP1 also targets HPIP, the loss of COP1 also leads to HPIP stabilization, which potentiates estrogens-dependent Akt activation. Both stabilized HPIP and c-Jun promote EMT. In these cells, the loss of COP1 also promotes Tamoxifen resistance. Therefore, COP1 acts as a tumor suppressor gene in these tumors.

Immunoprecipitations

HEK293 cells were washed twice with ice-cold PBS and lysed in 1 mL of IP buffer (Tris HCl 50 mM pH 8.0, NaCl 150 mM, NP-40 1%, EDTA 2 mM and protease inhibitors). Cells lysates were then centrifuged at 14,000 rpm at 4 °C for 10 minutes. The supernatant was collected and 100 μl of supernatant was used as an input. FLAG beads and mouse IgG agarose beads were washed three times with the immunoprecipitation (IP) buffer before being added to the lysates. Cell lysates were incubated overnight at 4 °C with FLAG beads or mouse IgG agarose beads. The next day, lysates were centrifuged at 2000 rpm at 4 °C for 5 minutes. The beads were washed three times with the IP buffer and subjected to Western blot analyses. For the detection of polyubiquitinated forms of HPIP, HEK293 cells were transfected with indicated plasmids and 24 hours later, cells were treated with MG132 at a final concentration of 20 μM for 2 hours before lysis. HEK293 cells were lysed in a denaturing lysis buffer (Tris HCl 50 mM pH 8.0, NaCl 150 mM, NP-40 1%, deoxycholate Na 0.5%, SDS 1%). Genomic DNA was sheared with a needle and a syringe and lysates were diluted 10 times in a dilution buffer (Tris HCl 50 mM pH 8.0, NaCl 150 mM, NP-40 1% with protease inhibitors) and incubated overnight at 4 °C with FLAG beads or mouse IgG agarose beads. FLAG and mouse IgG agarose beads were washed three times with dilution buffer before added to the lysates. 50 μl of undiluted lysates were used as an input. The samples were processed as for co-immunoprecipitation assays.

Immunofluorescence

Cells were seeded on coverslips in six-well plates. After treatment or not with Tamoxifen, cells were washed in PBS, fixed with 4% paraformaldehyde in PBS for 15 minutes and subsequently permeabilized with Triton-X100 0.2%/PBS for 10 minutes at room temperature. Cells were then washed and blocked for 1 hour (BSA 5% or normal goat serum 5% in PBS) followed by overnight incubation at 4 °C with primary antibodies. The next day, coverslips were incubated for 1 hour with appropriate goat secondary antibodies coupled to Alexa Fluor 488 or 568 fluorophores (Life Technologies), washed and incubated for 10 minutes with DAPI (Life Technologies). ProLong (Life Technologies) was used for mounting on glass slides and images were acquired with the Leica TCS SP5 II confocal system (Leica Microsystems, Wetzlar, Germany).

Real-time PCR analyses

mRNA isolation and quantifications were carried out as previously described [44]. Sequences of primers used in this study are listed in the Supplementary Table 2.

Transfections and lentiviral transductions

ShRNA control, -COP1, -Cullin 4A, -DDB1, -c-Jun, -DDB1, ERα and -HPIP lentiviral constructs were all from Sigma and are listed in Supplementary Table 3. Lentiviral infections of control or p53-deficient MCF7 cells with shRNA constructs where carried out as previously described [44]. Transient transfections of 293T cells were performed using the Mirus Bio TransIT-LT1 transfection reagent (Mirus Bio, Madison, WI, USA). For lentivirus-mediated shRNA experiments in MCF7 and ZR-75 cells, 3×10^6 LentiX 293 T cells were transfected with 12 µg of the "non-target" lentiviral shRNA plasmid ("Control") or with the shRNA constructs that target human COP1, DDB1, Cullin 4A, ERα or c-Jun, 12 µg of psPAX2 and 5 µg of VSVG plasmid, using the Mirus Bio TransIT-LT1 transfection reagent. The recombinant viruses were harvested 48 and 72 hours later. The virus particles containing supernatant was filtered through 0.45 µm PVDF membrane filters. MCF7 or ZR-75 cells were plated day before for final confluency 30% and supernatant containing virus was added. 24 hours later, the medium was changed with newly harvested lentiviral particles containing supernatant. The cells were split after 24 hours and incubated in puromycin-containing medium for 3 additional days.

Biochemical fractionation

Cells were trypsinized, washed twice with ice-cold PBS, resuspended and homogenized in a Dounce homogenizer with the lysis buffer (NaCl 150 mM, DTT 5 mM, EDTA 5 mM, Tris HCl 25 mM pH 7.4, protease inhibitors) and centrifuged at $1000 \times g$ for 10 minutes at 4 °C. The supernatant was adjusted to 1% Triton X-100 and left on ice for 30 minutes. Four volume of OptiPrep were added to two volume of supernatant. OptiPrep was diluted with the lysis buffer plus 1% Triton X-100 to give 30%, 25%, 20% and 5% (w/v) iodixanol. A total of 0.6 ml of each sample as well as the four gradient solutions were layered in tubes for swinging-bucket rotor. Samples were centrifuged at 30,000 rpm for 16 hours. Fractions of equal volume were collected for subsequent Western blot analyses.

Extraction of cytoplasmic and nuclear proteins

Cells were trypsinized, washed twice with PBS and incubated on ice for 10 minutes in the cytoplasmic lysis buffer (Tris HCl 10 mM pH 7.9, sucrose 340 mM, EDTA 0.1 mM, $CaCl_2$ 3 mM, $MgCl_2$ 2 mM, NP-40 0.5%, DTT 1 mM and protease inhibitor). After centrifugation at 3500 *g* for 15 minutes at 4 °C, the supernatant fraction (cytoplasmic extract) was harvested and the pellet was washed 5 times with the cytoplasmic lysis buffer without NP-40. After this step, the pellet was resuspended in nuclear lysis buffer (HEPES 20 mM pH 7.9, KOAc 150 mM, $MgCl_2$ 1.5 mM, EDTA 3 mM, Glycerol 10 %, DTT 1 mM, NP-40 0.1% and protease inhibitor), incubated on ice for 10 minutes, and centrifuged at 14,000 rpm for 5 minutes at 4 °C. The supernatant containing the nuclear fraction was retained.

ChIP assays

ChIP assays were carried out with extracts from control or COP1-depleted MCF7 cells. Cells were crosslinked for 10 minutes at room temperature (1/10th of the crosslinking mix was directly added to the plate containing the cells and the culture medium). The reaction was quenced by adding 1/10th of volume 1.25 M glycine to reach 125 mM of concentration. Cells were then washed twice with PBS and lysed with the lysis buffer (SDS 1%, EDTA 10 mM, pH 8.0, Tris-HCl 50 mM, pH 8.0 with protease inhibitors). Cells were harvested by scraping from the plates. Cell lysates were sonicated on ice for 15 minutes using the Bioruptor sonicator (Diagenode, Liege, Belgium). Lysates were then spin down for 5 minutes at maximum speed in a bench-top centrifuge and diluted ten times with the dilution buffer (Triton X-100 1%, NaCl 150 mM, EDTA 2 mM pH 8.0, Tris-HCl 20 mM pH 8.0 with protease inhibitors). 5 µg of antibody was added for each experimental condition and tubes were rotated overnight at 4 °C. Simultaneously, protein A or G beads were washed with the dilution buffer and pre-absorbed with 100 µg/ml BSA in rotating tubes overnight at 4 °C. The next day, beads were added to the IP mix and rotated for 1–2 hours at 4 °C. All beads were subsequently washed three times with the washing buffer (Triton X-100 1%, 0.1% SDS, NaCl 150 mM, EDTA 2 mM pH 8.0, Tris-HCl 20 mM pH 8.0 with protease inhibitors), once with the final washing buffer (Triton X-100 1%, SDS 0.1%, NaCl 500 mM, EDTA 2 mM pH 8.0, Tris-HCl 20 mM, pH 8.0 with protease inhibitors) and once with the washing buffer B (Tris 20 mM pH 8.0, EDTA 1 mM, LiCl 250 mM, NP-40 0.5 %, Na-deoxycholate 0.5 %, protease inhibitors). 450 µl of elution buffer (SDS 1%, $NaHCO_3$ 100 mM) were added to each IP reaction. For inputs, 400 µl of elution buffer were added to 50 µl of each lysate. Proteinase K and RNAse A (500 µg/ml each) were added to each reaction and incubated for 30 minutes at 37 °C. Samples were subsequently reverse cross-linked at 65 °C overnight (20 µl of 5 M NaCl were added prior the reverse crosslinking to each reaction). DNAs were purified using the phenol–chloroform extraction method, precipitated with Ethanol and resuspended in 100 µl of sterile water. 1 µl was used for PCR reactions. Sequences of primers used are listed in the Supplementary Table 2.

Cell cycle analyses by flow cytometry

The Click-iT® EdU 488 kit (Thermofisher) was used to assess the consequences of estrogen signaling on the cell cycle. Control and COP1-depleted MCF7 cells were treated or not at distinct time points and EdU (10 µM) was added in the growth media for 2 hours. The same population of cells which were not incubated with EdU were used as negative control. Cells were harvested, washed twice with 3 mL of 1% BSA in PBS and centrifuged. The resulting pellets were dislodged and 100 µL of Click-iT® fixative (Component D) was added. Cells were fixed for 15 minutes at room temperature. After fixation, cells were washed with 3 mL of 1% BSA in PBS and centrifuged. Pellets were permeabilized with 100 µL of 1X Click-iT® saponin-based permeabilization and wash reagent for 15 minutes. Cells were subsequently labeled using the Click-iT® reaction cocktail made-up using the following reagents (for 10 reactions): PBS, D-PBS or TBS (4.38 mL), $CuSO_4$ (Component F) (100 µL), Fluorescent dye azide (25 µL) and a reaction buffer additive (500 µL) for a total of 5 mL. 0.5 mL of Click-iT® reaction cocktail was added to each tube and mixed. Reactions were incubated for 30 minutes at room temperature, protected from light. Cells were subsequently washed once with 3 mL of 1% BSA in PBS and centrifuged. The DNA stain (7-AAD) in 1% BSA in PBS (200 µL) was added to each pellet and cells were analyzed by flow cytometry using FACS CANTO II.

Boyden chamber and collagen I invasiveness assays

For Boyden chamber assays, 1.5×10^4 control or depleted PyMT cells were seeded in each chamber in triplicates. 20 hours later, cells were fixed and stained with 30% methanol and 0.05% Crystal violet. Pictures of three random fields were taken for each chamber. The number of cells were calculated in each field with using the ImageJ software.

For collagen I invasiveness assays, mammospheres of control or COP1-depleted PyMT cells were grown as described for MCF7 cells. Once they reached a size of about 200 µm, they were collected by gentle centrifugation (1000 rpm for 5 minutes at room temperature). The medium was removed and they were plated in collagen (Collagen I from rat tail, ScienCell Research Laboratories, cat#8688), covered in growth media in 24 wells and grown for 24 hours. The invasiveness was calculated using the ImageJ Software.

Flow cytometry to assess the pool of cancer stem cells

Cells were trypsinized, collected with full media and centrifuged at 200 *g* for 5 minutes. After, cells were washed once with PBS. They were then diluted in 500 µl of PBS/1% BSA and incubated for 40 minutes on ice with the anti-human CD24-PE BD and CD44-Alexa 488 BD antibodies (Pharmingen), washed ones in PBS/1% BSA and analyzed on the FACS CANTOII.

Cell viability assay

Control or COP1-depleted MCF7 cells were counted and seeded (3000 cells per well) in 96 wells plates. Cells were treated with 5 µM Tamoxifen every other day. After 6 days of treatment, viable cells were counted using the Cell Counting Kit-8 (Sigma), according to the manufacturer's protocol (10 µl of solution in each well, keeping cells for 2 hours in the incubator and reading the absorbance at 450 nm).

Mammosphere formation assay

Control or COP1-depleted MCF7 cells were trypsinized in order to generate single cell suspension, washed two times with PBS, resuspended in complete mammosphere media, counted and seeded into Costar® 24-well Clear Flat

Bottom Ultra-Low Attachment Multiple Well Plates (5000 cells per well) and grown for 5 days before taking picture. The complete mammosphere media was DMEM/F12 supplemented with 2 mM L-glutamine, 100 U/mL penicillin, 100 U/mL streptomycin and immediately prepared before use by adding 20 ng/ml of recombinant human epidermal growth factor (EGF, Sigma), 10 ng/mL recombinant human basic fibroblast growth factor (bFGF, R&D Systems) and 1× B27 supplement (Thermo Fisher Scientific).

Establishment of the metabolomic profiles by targeted metabolomics

For targeted metabolomics analyses of control versus COP1-depleted MCF7 cells treated or not with estrogens, each sample was washed three times with chilled PBS collected into Eppendorf tube, freezed in liquid nitrogen and stored at −80 °C until extraction. Extraction solution used was 50% methanol, 30% ACN, and 20% water. The volume of extraction solution added was calculated from the cell count (2×10^6 cells per ml). After addition of extraction solution samples were vortexed for 5 minutes at 4 °C, and then centrifuged at 16,000 g for 15 minutes at 4 °C. The supernatants were collected and analyzed by liquid chromatography–mass spectrometry using SeQuant ZIC-pHilic column (Merck) for the liquid chromatography separation. Mobile phase A consisted of 20 mM ammonium carbonate plus 0.1% ammonia hydroxide in water. Mobile phase B consisted of ACN. The flow rate was kept at 100 ml/minute, and the gradient was 0 minute, 80% of B; 30 minutes, 20% of B; 31 minutes, 80% of B; and 45 minutes, 80% of B. The mass spectrometer (QExactive Plus Orbitrap, Thermo Fisher Scientific) was operated in full scan, polarity switching mode with the spray voltage set to 2.5 kV and the heated capillary held at 320 °C. The sheath gas flow was set to 20 units, the auxiliary gas flow to five units and the sweep gas flow to zero units. The metabolites were detected across a mass range of 75–1000 *m/z* at a resolution of 35,000 (at 200 *m/z*) with the automatic gain control target at 10^6 and the maximum injection time at 250 ms. Lock masses were used to ensure mass accuracy below 5 ppm. Data were acquired with the Thermo Xcalibur software (Thermo Fisher Scientific). The peak areas of metabolites were determined using the Thermo TraceFinder software (Thermo Fisher Scientific), identified by the exact mass of each singly charged ion and by the known retention time on the HPLC column. To obtain a robust statistical analysis, metabolomics data were normalized using the median normalization method [46]. The data were further pre-processed with a log transformation. The MetaboAnalyst 3.0 software [47] was used to conduct statistical analyses and heatmaps generation, and unpaired two-sample *t* test was chosen to perform the comparisons. The algorithm for heatmap clustering was based on the Pearson distance measure for similarity and the Ward linkage method for biotype clustering. Metabolites with similar abundance patterns were positioned closer together.

Extracellular flux assays

Oxygen consumption rate (OCR - pmol/min) measurements were performed with a Seahorse XFp extracellular flux analyzer (Agilent, Santa Clara, CA). Control or COP1-depleted MCF7 cells were grown in DMEM/F12 w/o phenol red supplemented with Charcoal/Dextran treated FBS (Hyclone/Fisher) for 48 hours. Next, cells were seeded in XFp mini-plates (Agilent) (15000 cells per well) in DMEM/F12 w/o phenol red supplemented with Charcoal/Dextran treated FBS (Hyclone/Fisher) and allowed to attach for 6 hours. Cells were then treated or not with E2 (10 nM) for 16 hours. Seahorse experiments were performed as previously described [48].

For mitochondrial OCR (pmol/min) analysis, cells were kept in unbuffered serum-free DMEM (Basal DMEM, Agilent w/o phenol red) supplemented with pyruvate (1 mM), glutamine (2 mM), glucose (10 mM), pH 7.4 at 37 °C, and ambient CO_2 for 1 hour before the assay. During the assay, cells were successively stressed with oligomycin (1 µM), FCCP (1.0 µM), and rotenone/antimycin A (0.5 µM each) mix. All results were normalized according to the cell number evaluated by Hoechst (2 µg/mL) incorporation after cold methanol/acetone fixation followed by a well-scanning. Results shown are representative ones out of three independent experiments. Two-sided statistical analysis was performed using one-way analysis of variance followed by Tukey's multiple comparisons. Graph for ECAR is shown with SEM error bars while SD is shown in all other graphs.

High-throughput RNA sequencing, pre-processing, and mapping

RNA sequencing was performed on libraries prepared from total RNA samples. Three biological replicates were analyzed for each condition. RNA integrity was verified on a Bioanalyser 2100 with RNA 6000 Nano chips (Agilent technologies, CA, USA). RNA integrity number score was above 9 for every sample. Libraries were prepared using Truseq® stranded mRNA Sample Preparation Kits (Illumina, CA, USA) following manufacturer's instructions. Libraries were validated using QIAxcel Advanced System and quantified by qPCR using the KAPA library quantification kit. Libraries were multiplexed and sequenced on an Illumina NextSeq500 sequencer to generate more than ~25,000,000 paired-end reads (2×150 bases) per library. Raw reads were demultiplexed and adapter-trimmed using Illumina bcl2fastq conversion software v2.20. Reads were processed within the nf-core/rnaseq-1.4.2 pipeline [49] using STAR aligner, the human reference genome GRCh38 and the gene annotations from Ensembl release 97. Quality of the sequencing data was successfully controlled using QC modules of the pipeline and a report has been compiled with MultiQC. The data has been deposited and the GEO accession number is GSE183753.

Differential expression analysis at the gene level

Counts matrice has been generated at gene level using *featureCounts*. Clustering, Principal Component Analysis and Differential Expression Analysis have been performed using the R package *DESeq2* [50]. Design for the differential expression analysis implies comparing samples deficient for COP1 to control samples at two different timepoints. Genes with an adjusted *p* values (Benjamini-Hochberg procedure corresponding to FDR) below 0.1 were considered significantly affected. Differentially expressed genes were evaluated for their dependance to one timepoint or the other. This was visualized through fold change plot and genes were classified using their significance in both comparisons.

Statistical analyses

All graphs, calculations and statistical analyses were performed using the GraphPad Prism Software, version 8.0 (GraphPad software, San Diego, CA, USA). The comparison of medians between different groups was done using the one-way ANOVA followed by Tukey's multiple comparisons post-hoc test. For two-way ANOVA tests, the Bonferroni's test was used as post-hoc test.

REFERENCES

1. Craig Allred D, Brown P, Medina D. The origins of estrogen receptor alpha-positive and estrogen receptor alpha-negative human breast cancer. Breast Cancer Res. 2004;6:240–5.
2. Rae JM, Johnson MD, Scheys JO, Cordero KE, Larios JM, Lippman ME. GREB1 is a critical regulator of hormone dependent breast cancer growth. Breast Cancer Res Treat. 2005;92:141–9.
3. Ikeda K, Horie-Inoue K, Inoue S. Identification of estrogen-responsive genes based on the DNA binding properties of estrogen receptors using high-throughput sequencing technology. Acta Pharmacol Sin. 2015;36:24–31.
4. Welboren WJ, Van Driel MA, Janssen-Megens EM, Van Heeringen SJ, Sweep FC, Span PN, et al. ChIP-Seq of ERα and RNA polymerase II defines genes differentially responding to ligands. EMBO J. 2009;28:1418–28.
5. Welboren WJ, Sweep FCGJ, Span PN, Stunnenberg HG. Genomic actions of estrogen receptor α: What are the targets and how are they regulated? Endocr-Relat Cancer. 2009;16:1073–89.
6. Folkerd EJ, Dowsett M. Influence of sex hormones on cancer progression. J Clin Oncol. 2010;28:4038–44.
7. Koš M, Reid G, Denger S, Gannon F. Minireview: genomic organization of the human ERα gene promoter region. Mol Endocrinol. 2001;15:2057–63.
8. Yoshida T, Eguchi H, Nakachi K, Tanimoto K, Higashi Y, Suemasu K, et al. Distinct mechanisms of loss of estrogen receptor α gene expression in human breast cancer: Methylation of the gene and alteration of trans-acting factors. Carcinogenesis. 2000;21:2193–201.
9. Turner BC, Zhang J, Gumbs AA, Maher MG, Kaplan L, Carter D, et al. Expression of AP-2 transcription factors in human breast cancer correlates with the regulation of multiple growth factor signalling pathways. Cancer Res. 1998;58:5466–72.
10. Grabinski N, Möllmann K, Milde-Langosch K, Müller V, Schumacher U, Brandt B, et al. AKT3 regulates ErbB2, ErbB3 and estrogen receptor α expression and contributes to endocrine therapy resistance of ErbB2+ breast tumor cells from Balb-neuT mice. Cell Signal. 2014;26:1021–9.
11. Madureira PA, Varshochi R, Constantinidou D, Francis RE, Coombes RC, Yao KM, et al. The forkhead box M1 protein regulates the transcription of the estrogen receptor α in breast cancer cells. J Biol Chem. 2006;281:25167–76.
12. Eeckhoute J, Keeton EK, Lupien M, Krum SA, Carroll JS, Brown M. Positive cross-regulatory loop ties GATA-3 to estrogen receptor α expression in breast cancer. Cancer Res. 2007;67:6477–83.

13. Doucas V, Spyrou G, Yaniv M. Unregulated expression of c-Jun or c-Fos proteins but not Jun D inhibits oestrogen receptor activity in human breast cancer derived cells. EMBO J. 1991;10:2237–45.
14. Smith LM, Wise SC, Hendricks DT, Sabichi AL, Bos T, Reddy P, et al. cJun overexpression in MCF-7 breast cancer cells produces a tumorigenic, invasive and hormone resistant phenotype. Oncogene. 1999;18:6063–70.
15. Tecalco-Cruz AC, Ramírez-Jarquín JO. Mechanisms that increase stability of estrogen receptor alpha in breast cancer. Clin Breast Cancer. 2017;17:1–10.
16. Manavathi B, Acconcia F, Rayala SK, Kumar R. An inherent role of microtubule network in the action of nuclear receptor. Proc Natl Acad Sci USA. 2006;103:15981–6.
17. Shostak K, Patrascu F, Göktuna SI, Close P, Borgs L, Nguyen L, et al. MDM2 restrains estrogen-mediated AKT activation by promoting TBK1-dependent HPIP degradation. Cell Death Differ. 2014;21:811–24.
18. Marine JC. Spotlight on the role of COP1 in tumorigenesis. Nat Rev Cancer. 2012;12:455–64.
19. Migliorini D, Bogaerts S, Defever D, Vyas R, Denecker G, Radaelli E, et al. Cop1 constitutively regulates c-Jun protein stability and functions as a tumor suppressor in mice. J Clin Investig. 2011;121:1329–43.
20. Vitari AC, Leong KG, Newton K, Yee C, Oğrourke K, Liu J, et al. COP1 is a tumour suppressor that causes degradation of ETS transcription factors. Nature. 2011;474:403–8.
21. Baert JL, Monte D, Verreman K, Degerny C, Coutte L, De Launoit Y. The E3 ubiquitin ligase complex component COP1 regulates PEA3 group member stability and transcriptional activity. Oncogene. 2010;29:1810–20.
22. Wertz IE, O'Rourke KM, Zhang Z, Dornan D, Arnott D, Deshaies RJ, et al. Human De-etiolated-regulates c-Jun by assembling a CUL4A ubiquitin ligase. Science. 2004;303:1371–4.
23. Dornan D, Wertz I, Shimizu H, Arnott D, Frantz GD, Dowd P, et al. The ubiquitin ligase COP1 is a critical negative regulator of p53. Nature. 2004;429:86–92.
24. Lorent J, Kusnadi EP, Hoef V, Rebello RJ, Leibovitch M, Ristau J, *et al*. Translational offsetting as a mode of estrogen receptor α-dependent regulation of gene expression. EMBO J. 2019;38. https://doi.org/10.15252/embj.2018101323.
25. Neeman M, Degani H. Metabolic studies of estrogen-and tamoxifen-treated human breast cancer cells by nuclear magnetic resonance spectroscopy. Cancer Res. 1989;49:589–94.
26. Neeman M, Degani H. Early estrogen-induced metabolic changes and their inhibition by actinomycin D and cycloheximide in human breast cancer cells: 31P and 13C NMR studies. Proc Natl Acad Sci USA. 1989;86:5585–9.
27. O'Mahony F, Razandi M, Pedram A, Harvey BJ, Levin ER. Estrogen modulates metabolic pathway adaptation to available glucose in breast cancer cells. Mol Endocrinol. 2012;26:2058–70.
28. Jia M, Andreassen T, Jensen L, Bathen TF, Sinha I, Gao H, et al. Estrogen receptor a promotes breast cancer by reprogramming choline metabolism. Cancer Res. 2016;76:5634–46.
29. van Gastel N, Stegen S, Eelen G, Schoors S, Carlier A, Daniëls VW, et al. Lipid availability determines fate of skeletal progenitor cells via SOX9. Nature. 2020;579:111–7.
30. Shostak K, Zhang X, Hubert P, Göktuna SI, Jiang Z, Klevernic I, et al. NF-κB-induced KIAA1199 promotes survival through EGFR signalling. Nat Commun. 2014;5. https://doi.org/10.1038/ncomms6232.
31. Mani SA, Guo W, Liao MJ, Eaton EN, Ayyanan A, Zhou AY, et al. The epithelial-mesenchymal transition generates. Cells Prop Stem Cells Cell. 2008;133:704–15.
32. Luque-Bolivar A, Pérez-Mora E, Eugenia Villegas V, Rondon-Lagos M. Resistance and overcoming resistance in breast cancer. Breast Cancer. 2020;12:211–29.
33. Cook KL, Shajahan AN, Wärri A, Jin L, Hilakivi-Clarke LA, Clarke R. Glucose-regulated protein 78 controls cross-talk between apoptosis and autophagy to determine antiestrogen responsiveness. Cancer Res. 2012;72:3337–49.
34. Samaddar JS, Gaddy VT, Duplantier J, Thandavan SP, Shah M, Smith MJ, et al. A role for macroautophagy in protection against 4-hydroxytamoxifen-induced cell death and the development of antiestrogen resistance. Mol Cancer Ther. 2008;7:2977–87.
35. Meley D, Bauvy C, Houben-Weerts JHPM, Dubbelhuis PF, Helmond MTJ, Codogno P, et al. AMP-activated protein kinase and the regulation of autophagic proteolysis. J Biol Chem. 2006;281:34870–9.
36. Kim J, Kundu M, Viollet B, Guan KL. AMPK and mTOR regulate autophagy through direct phosphorylation of Ulk1. Nat Cell Biol. 2011;13:132–41.
37. Chan EYW, Kir S, Tooze SA. siRNA screening of the kinome identifies ULK1 as a multidomain modulator of autophagy. J Biol Chem. 2007;282:25464–74.
38. Zou S, Zhu Y, Wang B, Qian F, Zhang X, Wang L, et al. The ubiquitin ligase COP1 promotes glioma cell proliferation by preferentially downregulating tumor suppressor p53. Mol Neurobiol. 2017;54:5008–16.
39. Wang SC, Chai DSen, Chen CB, Wang ZY, Wang L. HPIP promotes thyroid cancer cell growth, migration and EMT through activating PI3K/AKT signaling pathway. Biomed Pharmacother. 2015;75:33–39.
40. Ouyang M, Wang H, Ma J, Lü W, Li J, Yao C, et al. COP1, the negative regulator of ETV1, influences prognosis in triple-negative breast cancer. BMC Cancer. 2015;15. https://doi.org/10.1186/s12885-015-1151-y.
41. Lundberg AS, Weinberg RA. Functional inactivation of the retinoblastoma protein requires sequential modification by at least two distinct cyclin-cdk complexes. Mol Cell Biol. 1998;18:753–61.
42. Vega S, Morales AV, Ocaña OH, Valdés F, Fabregat I, Nieto MA. Snail blocks the cell cycle and confers resistance to cell death. Genes Dev. 2004;18:1131–43.
43. Hawley SA, Ross FA, Chevtzoff C, Green KA, Evans A, Fogarty S, et al. Use of cells expressing γ subunit variants to identify diverse mechanisms of AMPK activation. Cell Metab. 2010;11:554–65.
44. Shostak K, Jiang Z, Charloteaux B, Mayer A, Habraken Y, Tharun L, et al. The X-linked trichothiodystrophy-causing gene RNF113A links the spliceosome to cell survival upon DNA damage. Nat Commun. 2020;11. https://doi.org/10.1038/s41467-020-15003-7.
45. Gatot JS, Gioia R, Chau TL, Patrascu F, Warnier M, Close P, et al. Lipopolysaccharide-mediated interferon regulatory factor activation involves TBK1-IKKε-dependent lys63-linked polyubiquitination and phosphorylation of TANK/I-TRAF. J Biol Chem. 2007;282:31131–46.
46. Hendriks MMWB, Smit S, Akkermans WLMW, Reijmers TH, Eilers PHC, Hoefsloot HCJ, et al. How to distinguish healthy from diseased? Classification strategy for mass spectrometry-based clinical proteomics. Proteomics. 2007;7:3672–80.
47. Xia J, Sinelnikov IV, Han B, Wishart DS. MetaboAnalyst 3.0-making metabolomics more meaningful. Nucleic Acids Res. 2015;43:W251–W257.
48. Rademaker G, Hennequière V, Brohée L, Nokin MJ, Lovinfosse P, Durieux F, et al. Myoferlin controls mitochondrial structure and activity in pancreatic ductal adenocarcinoma, and affects tumor aggressiveness. Oncogene. 2018;37:4398–412.
49. Ewels PA, Peltzer A, Fillinger S, Patel H, Alneberg J, Wilm A, et al. The nf-core framework for community-curated bioinformatics pipelines. Nat Biotechnol. 2020;38:276–8.
50. Love MI, Huber W, Anders S. Moderated estimation of fold change and dispersion for RNA-seq data with DESeq2. Genome Biol. 2014;15. https://doi.org/10.1186/s13059-014-0550-8.

ACKNOWLEDGEMENTS

The authors thank Arnaud Blomme (Laboratory of Cancer Signaling, University of Liege, Liege, Belgium) for the gift of PyMT cells. The authors also thank the GIGA Imaging and Flow Cytometry Facility as well as the GIGA Genomics Platform for RNA-Sequencing analyses. This study was supported by Grants from the Belgian National Funds for Scientific Research (FNRS) and from Special Research Funds (FSR) at the University of Liege, the Belgian foundation against Cancer (FAF-F/2016/794), as well as from the Walloon Excellence in Life Sciences and Biotechnology (WELBIO-CR-2015A-02). We are also grateful to the "Fondation Leon Fredericq" of the CHU Liege for its financial support. A. Chariot and P. Close are Research Director and Senior Research Associate at the FNRS, respectively. The authors declare no conflict of interest.

AUTHOR CONTRIBUTIONS

Conceptualization, AC and KS; Methodology, SCT, QL, OP, PCh, AL, A M, PAF, PCl, SK, AF and IN; Investigation, SCT, QL, PCh, AL, AM, PAF, PCl, SK, AF and IN; Formal Analysis: SCT, OP, KS and AC; Writing—Original Draft, AC; Funding Acquisition, AC; Resources, RB; Supervision, AC.

COMPETING INTERESTS

The authors declare no competing interests.

ADDITIONAL INFORMATION

Supplementary information The online version contains supplementary material available at https://doi.org/10.1038/s41388-021-02038-3.

Correspondence and requests for materials should be addressed to Alain Chariot.

Reprints and permission information is available at http://www.nature.com/reprints

Publisher's note Springer Nature remains neutral with regard to jurisdictional claims in published maps and institutional affiliations.